AALBORG UNIVERSITY

MODELLING OF RANDOM VARIATIONS IN SOIL PROPERTIES

Master Thesis

MARTA MARTON
WEERAPONG PENRIYA

HANDED IN:
08/06/2015

SCHOOL OF ENGINEERING AND SCIENCE

Marta Marton and Weerapong Penriya

Frontpage picture by
This report is typeset in Times New Roman 11pt.
Layout and typography by the authors using LaTeX.

AALBORG UNIVERSITY
STUDENT REPORT

The School of Engineering and Science
Department of Civil Engineering
Sofiendalsvej 9-11, 9220 Aalborg Ø
Phone: 9940 8484
http://www.ses.aau.dk

Title:

Modelling of Random Variations in Soil Properties

Project period:

Spring Semester 2015

Supervisor:

Lars V. Andersen

Participants:

Marta Marton

Weerapong Penriya

Editions: 4
Report pages: 72
Appendix pages: 4
Completed: 08-06-2015

Synopsis:

The purpose of this project is to model the uncertainties, random variations in soil properties on the basis of random field theory, where the soil is modelled as a heterogeneous material.

Two-dimensional cross-correlated random fields are generated for the undrained shear strength and Young's modulus of the soil. After that a number of Monte Carlo simulations are performed and a catalogue of bearing capacities are obtained.

Based on the probability density function of the load and the resistance a reliability analysis is performed, by the crude Monte Carlo simulation technique and the partial safety factor for the undrained shear strength is calibrated corresponding to a target reliability. This whole procedure is performed on two different geotechnical cases: a strip footing and an embankment.

Preface

This thesis is a product of two students' project work at the 4th semester of the Master Programme in Structural and Civil Engineering at the School of Engineering and Science at Aalborg University, under the supervision of Lars V. Andersen. The project is completed within the period 1st of February to 8th of June 2015. The thesis is prepared and made in compliance with the current curriculum of the 4th semester in M.Sc. Structural and Civil Engineering.

Reading Guide

The references located within the paper are stated in the Bibliography, at the end of this report. For this purpose the Harvard method was used. The Harvard referencing system shows authors surname and the publication year. This source is placed on a current place across the paper and refers to the Bibliography at the end of the report, where the reference is completed. The completed reference states the following: author, title, edition, publisher and year of publication. Web pages are listed with authors, title, web sites URL address, publish year and date of downloading.

The thesis consists of three parts: a main report, an appendix, which are found in the back of the report, and an electronic appendix on an attached CD. The main report refers to the appendix and CD, where the appertaining calculations and extensional documents are to be found. The files used in the different software, e.g. Matlab , Python and Fortran, are attached to the electronic appendix CD. All references to the appendixes starts with an Arabic letter. For example the first section in appendix A is thus to be referred to as Appendix A.1.

The following programmes are used for calculations and simulations throughout the thesis: Matlab, Fortran, Abaqus.

Summary

Geotechnical data is constrained with uncertainties. Among them is the natural variability of the soil which is a type of uncertainty that cannot be reduced. When designing a structure, this unpredictability of the soil has to be taken into account. The traditional way of doing this is based on a deterministic design, where partial safety factors are applied to the characteristic value of the loads and strength parameters, leading to a design based on increased loads and decreased strengths.

The purpose of the thesis is to model the random variations in soil properties using a probabilistic approach, based on the random field theory, in which soil properties are characterized in terms of their means and standard deviations, and through a realiability analysis to calibrate the partial safety factor for the undrained shear strength. The partial safety factor in Denmark is set to $\gamma_{cu} = 1.8$, which is quite high compared to the general factor proposed in Eurocode 7, $\gamma_{cu} = 1.4$.

Two-dimensional cross-correlated random fields for the undrained shear strength and Young's modulus of the soil are generated based on the matrix decomposition method. The probabilistic finite element model is created by using different packages; Abaqus, Python scripts, Fortran subroutines and Matlab scripts. 1000 Monte Carlo simulations are performed, resulting in 1000 bearing capacities of the structure. The data is then fitted and combined with the probability density function of the load a number of realizations are performed with the crude Monte Carlo simulation technique. Through this the partial safety factor of the undrained shear strength is calibrated to a corresponding target reliability index. This whole procedure is performed for two examples, one for a strip footing and one for an embankment.

The reliability-based calibration shows that the partial safety factor can be reduced significantly, from $\gamma_{cu} = 1.8$ to $\gamma_{cu} = 1.5$, in both cases, by which the costs are reduced too.

In addition, the effects of the correlation length on the failure mechanism is investigated, and it is found that the failure mechanism is highly dependent on the correlation length.

Contents

CHAPTER 1

Introduction

The soil data used in geotechnical design are usually associated with uncertainty. These uncertainties can come from the natural variability of the soil, but also from uncertainties related to imperfect knowledge, such as statistical, model and measurement uncertainty. In this project the main focus will be set on the natural variability of the soil, which is a type of uncertainty that cannot be reduced. The traditional way to deal with these uncertainties is based on a deterministic design, where the soil is modelled as a locally homogeneous material within each soil layer, resulting in a symmetric failure mechanism (Terzaghi), as seen on Figure 1.1. Here partial safety factors are applied to the characteristic values of material properties and loads. But if these partial safety factors are not chosen carefully, the structure could end up being too safe, and thus very expensive. One way to reduce these costs is a reliability-based calibration of the partial safety factors which corresponds to a well defined target reliability, depending on the type of structure and the characteristics of the considered failure mode. In the reliability analysis, probabilistic models are used, where the soil is modelled as a heterogeneous material, resulting in a random failure mechanism, as seen in Figure 1.2.

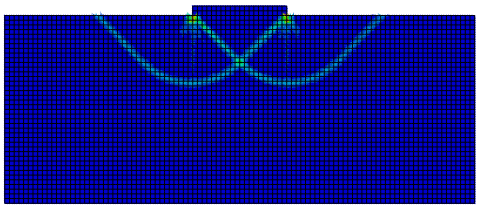

Figure 1.1: Deterministic design.

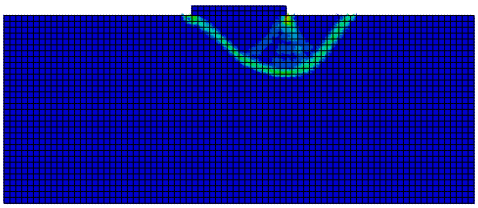

Figure 1.2: Probabilistic design.

Currently in Denmark the partial safety factor for the undrained shear strength is set quite high, $\gamma_{cu} = 1.8$, compared to the general factor proposed in Eurocode 7, $\gamma_{cu} = 1.4$. This will introduce a very high cost, and therefore it is of interest to investigate, if the value of 1.8 is really necessary.

The purpose of this project is to model the uncertainties, random variations in soil properties with the use of finite element method on the basis of random field theory, where the soil is modelled as a heterogeneous material, even within a single layer. In the random field theory all the parameters are modelled by stochastic variables characterized by a well chosen distribution function, a mean value, coefficient of variation and corre-

lation lengths. The effect of different correlation lengths on the failure mechanism will be investigated, as this differs significantly from the homogeneous one. After the probabilistic model of the soil and load is described and constructed, a reliability analysis will be performed, based on the crude Monte Carlo simulation technique, and the partial safety factor for the undrained shear strength will be calibrated corresponding to a target reliability. This whole procedure will be performed on two different geotechnical cases: a strip footing and an embankment.

1.1 Thesis Statement

Through the topics presented in the introduction it is desired to answer the following question:

Can the partial safety factor of the undrained shear strength be reduced through a reliability-based calibration, compared to the value specified in the Danish National Annex to DS/EN 1997-1 [2007], Eurocode 7.

1.2 Delimitation of Thesis

The main focus of the thesis is set on the spatial variation of the soil properties, therefore the model, measurement and statistical uncertainty will not be treated.

In order to model the variations of the soil properties two random fields were generated: one for the undrained shear strength and one for the Young's modulus of the soil.

In the thesis only cohesive soils are considered. Both the undrained shear strength and Young's modulus are assumed to have a lognormal distribution. The characteristic value of the undrained shear strength will be taken as a 95% confidence level of the mean strength. As no soil data was available, the characteristic values are assumed to have a certain value, which are typical values for clayey soils. The coefficient of correlation between the two random fields is assumed to take the value of 0.9

The load applied on the structure is a uniformly distributed load, directed downward vertically. The characteristic value of the load is taken as 98% quantile and a Gumbel distribution is assumed.

As no data was available, the coefficient of variation for the undrained shear strength and load are taken as 40%. The values for the different correlation lengths are also assumed.

The covariance matrix between the undrained shear strength and Young's modulus assumes an ellipsoidal Markovian structure.

Only the ultimate limit state (ULS) analysis is performed, meaning that the deformations will be not investigated, so serviceability limit state (SLS) is not considered.

The main focus is set to the embankment, the footing model mainly served as a simplification and validation, which was later modified to the embankment model.

These delimitations are of general concern throughout the thesis. Additional and more specific delimitations will be presented in the appropriate chapters and sections.

1.3 Overview of the Thesis

The thesis is divided into two main parts with Part I devoted to theory and Part II to practice.

Part I - Theory

- Chapter 2 introduces the various uncertainties related to the soil, and describes how variation of soil properties occurs in reality and how these uncertainties are modelled. A discussion is also included about the characteristic value of the soil properties and how the 95% confidence level of the mean strength is found.
- Chapter 3 introduces the random field theory, based on which the variation of soil properties are modelled. Here the characteristics and assumptions needed to define a Gaussian and stationary random field are listed and described in details. Further on the matrix decomposition method is presented, which was used in order to create the two-dimensional cross correlated random fields, one for the undrained shear strength and one for the Young's modulus of the soil.
- In Chapter 4 the procedure to construct the probabilistic finite element model is described, along with the description of the material model and the finite mesh used in the models. This chapter includes also a description on how the load was modelled.
- Chapter 5 introduces the reliability analysis and how this was performed in this thesis. Then the crude Monte Carlo simulation technique is presented. Finally the target reliabilities are defined and the whole workflow is described, which gives a good overview on the calculation steps.

Part II - Practice

- Chapter 6 presents the footing example, where the geometry and all the parameters used in the probabilistic model are presented. Further on analytical calculations are shown, along with a convergence analysis. In the end the results are presented, which include the calibrated partial safety factors based on the reliability analysis. In addition the effects of the correlation length on the failure mechanism are described and discussed.
- Chapter 7 presents the embankment example, which follows the same structure as Chapter 6. After the problem is well presented the results are shown and discussed.

Part I

Theory

CHAPTER 2

Uncertainties

In engineering the presence of uncertainty is unavoidable. The available data are sometimes incomplete or insufficient and they might invariably contain variability. Apart from this, engineers also rely on assumptions or estimations based on models which contain uncertainties as well. These uncertainties are usually divided into two main types, namely aleatory and epistemic uncertainties. The aleatory uncertainty consists of physical uncertainty, and it is associated with the randomness of the phenomena in question, such as the natural variability of soil. On the other hand, the epistemic uncertainty is related to imperfect models of the real world, thanks to insufficient or imperfect knowledge of the reality. The epistemic uncertainties include statistical, model and measurement uncertainty. [DNV, 2012]

As this projects main focus is set to the uncertainties related to soil, in the following these are described in detail.

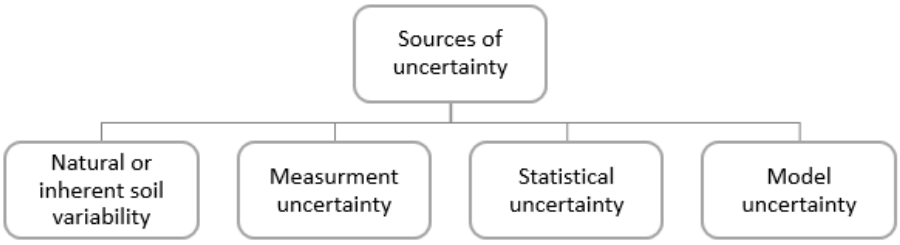

Figure 2.1: Sources of uncertainties in soils.

Natural or inherent soil variability

Natural or inherent soil variability is a physical uncertainty and it is the natural variation in a soil layer. This natural variability can be either continuous or discrete. Continuous spatial variability of a soil unit is characterized by an average trend of variation. A common example is the strength of the soil, which can increase with depth. But even continuous spatial variability is sometimes mixed with dislocation, like faults, lenses or fills. This comes from the natural formation of soil. This type of physical uncertainty is interpreted as discrete spatial variability. Such uncertainties cannot be reduced. [JCSS-C1, 2006]

Measurement uncertainty

In order to get information about the subsurface conditions, field investigation is required. The information can be gathered by the use of bore holes, cone penetration tests (CPT) or geophysical records. During these tests and site investigations uncertainties can arise due to imperfect measurements and/or sample disturbance. Strictly sticking to testing standards with sufficiently accurate measuring devices these uncertainties can be reduced by collecting more samples, performing more tests or employing more accurate methods of measurements. [JCSS-C1, 2006]

Statistical uncertainty

Soil data generally is only available for a small part of the soil, as usually the number of observations and samples is of limited amount. This will result in uncertainties that are of statistical nature. The limited data will not give reliable estimates for the distribution and autocorrelation functions. This type of uncertainties can be reduced by collecting more data.

Model uncertainty

Typically, the measured tests, observations have to be modified in order for the data to be suitable for design. These modifications rely on assumptions or estimations, which already carry uncertainties. The model uncertainties can come from imperfect engineering models, wrong choices of probability distribution and autocorrelation functions and/or characteristic values.

This project is focusing on the natural randomness, variability of the soil properties, and the uncertainties related to the choice of probability distribution and autocorrelation functions are not going to be considered. The uncertainties coming from the definition of characteristic value of soil properties are disregarded as well.

2.1 Soil Variability

Natural variability occurs in soil, both horizontally and vertically, meaning that its properties vary from place to place within resulting deposits, and it is different from field to field. This variability can be explained by the natural geological processes such as weathering, erosion and sedimentation processes. Additionally, soils have been subjected to various stresses, pore fluids, and physical and chemical changes, which is also an explanation for the variability. This natural variability can be further increased by human disturbance, in particular through erosion and gullying which can increase soil variability through the remixing of sediments and exposure of underlying sediments by gully dissection. [C.Fitzjohn et al., 2002]

2.2 Modelling the Variation of Soil Properties

The spatial variability of soil properties is difficult to predict deterministically. The limited sampling makes this even harder. Several mathematical models have been proposed to model the variation of soil properties. In general two main approaches can be distinguished: standard statistical and geostatistical.

Performing standard statistical analysis on a set of samples from a site investigation might show that the values of the measured strength of the soil can be described by a certain distribution type, but this will not give any information about which soil part has higher values and which one low ones. One way to avoid this, is applying geostatistical analysis, which in addition to the distribution type of the soil property gives also information about the spatial variability. Geostatistics is a tool to show, for example, how the undrained shear strength varies with depth, predicting the zones with higher and lower values. [Davidović et al., 2010]

One of the common methods among geostatistics includes kriging and simulation of random fields. Kriging is an estimation technique which, based on known (measured) values of soil parameters in conjunction with the autocorrelation function, makes it possible to estimate the soil properties in positions where no measurements have been performed. [DNV, 2012]

On the other hand, a random field is a list of random numbers whose location are mapped onto a space. These random numbers are generated based on different methods, in which the values of the random numbers are often spatially correlated in one way or another. The random field theory is further explained in Chapter 3, as in this project this method was adapted in order to model the random variation of soil properties.

2.3 Characteristic Value of Soil Properties

As it was explained earlier there are various types of uncertainties which can be present in loading, material properties and other aspects of any structure. But to design these structures all the uncertainties involved must be taken into account. In most of the engineering projects, dealing with these uncertainties is based on deterministic design. This means, that partial safety factors are applied to the characteristic values of loads and material properties. As a result, the whole design is based on increased loads and decreased strengths. It is of great importance, to note that, because of this, the reliability of the final design is highly dependent not only on the partial factors used but also on the manner in which the characteristic value has been chosen and assessed.

There are different ways of defining the characteristic value of a soil property. DNV [2012] states that the chosen definition of the characteristic value usually depends on the design code which is to be applied and of course on the actual problem. Some of these definitions which are often used are:

- mean value of the shear strength
- 5% quantile of the strength distribution
- 95% confidence level of the mean strength

For problems which are governed by a local soil strength a 5% quantile value of the strength is usually chosen as the characteristic value. For problems where large soil volumes are involved, the mean value is often taken as the characteristic value, as the local strength variations are assumed to average out. DS/EN 1997-1 [2007] suggests that the characteristic value shall be taken as a ”conservatively assessed mean value”, meaning that the characteristic value should be taken with a confidence of 95%.

In this project the characteristic value of the undrained shear strength will be taken as the 95% confidence level of the mean shear strength.

2.3.1 95% confidence level for the mean strength

In the following it is described how the characteristic value of the shear strength can be found as a 95% confidence level for the corresponding mean value.

The characteristic value of the undrained shear strength, c_{uk}, can be described by Equation (2.1):

$$c_{uk} = \mu_{cu} - f\frac{\sigma_{cu}}{\sqrt{n}} \tag{2.1}$$

where,

c_{uk}	characteristic value of the undrained shear strength
μ_{cu}	mean undrained shear strength
f	statistical coefficient related to the type of distribution, confidence limits and number of test values
n	number of samples

The mean strength, μ_{cu}, can be estimated by the sample mean:

$$\mu_{cu} = \frac{1}{n}\sum_{i=1}^{n} c_{u,i} \tag{2.2}$$

The standard deviation, σ_{cu}, is estimated by the sample standard deviation:

$$\sigma_{cu} = \sqrt{\frac{1}{n-1}\sum_{i=1}^{n}\left(c_{u,i} - \mu_{cu}\right)^2} \tag{2.3}$$

If the coefficient of variation, $COV_{cu} = \sigma_{cu}/\mu_{cu}$, is substituted into Equation (2.1), this will lead to:

$$c_{uk} = \mu_{cu}\left(1 - \frac{f}{\sqrt{n}}COV_{cu}\right) \tag{2.4}$$

Several approximations and simplifications were proposed of Equation (2.1). Some of them are presented in the following.

Based on Equation (2.1) Student [1908] proposed for the characteristic value to be defined as:

$$c_{uk}^{Student} = \mu_{cu} - t_{0.95,n-1}\frac{\sigma_{cu}}{\sqrt{n}} \tag{2.5}$$

Here, $t_{\alpha,\nu}$ is the inverse of Student's t cumulative distribution function with $\nu = n-1$ degrees of freedom for non-exceedance probability α.

Ovesen [1995] simplified Student's equation and arrived to the following:

$$c_{uk}^{Ovesen} = \mu_{cu} - 1.645\frac{\sigma_{cu}}{\sqrt{n}} \tag{2.6}$$

Based on comparative computations, Schneider [1999] also proposed a good approximation to Equation (2.4):

$$\frac{f}{\sqrt{n}} \cong \frac{1}{2} \tag{2.7}$$

Schneider's simplification leads to characteristic values within reasonable accuracy, can be applied to typical distribution types for soil (normal or lognormal) and it is applicable even when no test values are available. As in this project this is the case, it is reasonable to use Schneider's equation.

Schneider's proposed relationship for determination of the characteristic value of the shear strength as a 95% confidence level for the corresponding mean value is defined in Equation (2.8).

$$c_{uk}^{Schneider} = \mu_{cu} - 0.5\sigma_{cu} \tag{2.8}$$

It should be noted, that from now on $c_{uk}^{Schneider}$ will be noted as c_{uk}.

As this project will have the coefficient variation as an input parameter, it is more advantageous to write Schneider's equation in terms of the coefficient of variation instead of the standard deviation, as seen in Equation (2.9).

$$c_{uk} = \mu_{cu}\,(1 - 0.5COV_{cu}) \tag{2.9}$$

CHAPTER 3

Random Fields

Soil deposits are constrained with spatial variability (uncertainty), meaning that the soil varies from one location to another, even if it is the same soil type. This might be a result of natural geological processes or engineering construction. This chapter focuses on how this spatial variability of soil properties can be modelled as a random field. The characteristics and assumptions of random fields are described, together with how the random fields are generated.

3.1 Characteristics and Assumptions

An important characteristic of a random field is the concept of statistical dependence between field values at different points. From the mathematical viewpoint a random field can be interpreted as a two or three dimensional random process. Specifically, a two dimensional random field, $X(x,y)$ is a set of random variables, X_1,X_2, ..., each associated with the value of a certain property of interest (for example undrained shear strength) at the points (x_1,y_1), (x_2,y_2), ... in the field. In general, a random field may be defined by:

- its mean, μ, which gives information about its central tendency,
- its standard deviation, σ, which is a measure of the spread or scatter about the mean,
- its dimensionless coefficient of variation, COV, defined as the ratio of the standard deviation to the mean:
$$COV = \frac{\sigma}{\mu},$$
- its correlation function, ρ,
- its complete multivariate joint probability density function (PDF), which is the complete probabilistic description of all the points in the field from which probability calculations can be made.

A common way to exemplify the spatial variability is by plotting the variation of tip resistance measured over the soil depth during a cone penetration test (CPT), as seen in Figure 3.1. A CPT measurement can be thought as a continuous-state random process,

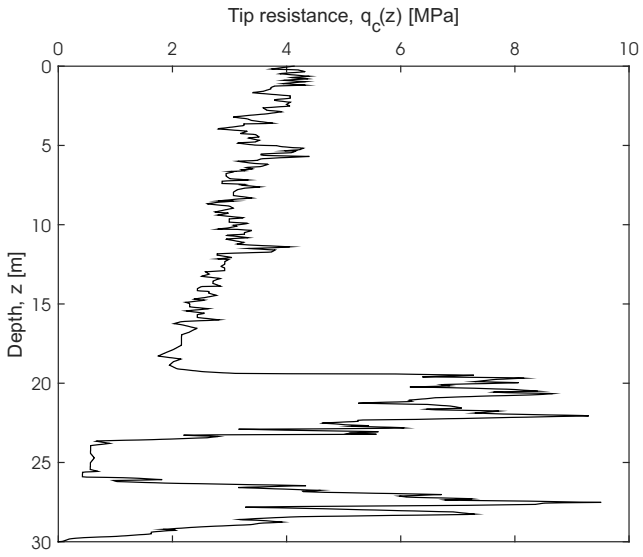

Figure 3.1: Tip resistance measured over the depth of the soil by a cone penetrometer.

where the random process $X(z)$ can take on an infinite number of possible outcomes at each point z.

The soil properties taken from this CPT can be constrained with measurement and/or model uncertainties, but apart from that, Figure 3.1 can give a reasonably good idea about the soil properties and soil types at the location where the CPT was performed. This of course gives information only at the location of the CPT, but there is no guarantee of having the same properties 10 or 50 m away from the CPT sounding. But by probabilistic methods the variability at the location where the CPT was performed can be used to represent the variability at other locations. [Fenton and Griffiths, 2008]

Spatial variability is characterized by variability at a point, which means that a different probability density function must be considered at each location of the soil unit. Another characteristic of spatial variability is the spatial dependence, meaning that two random variables will exhibit some dependence on each other, giving rise to joint probability distributions. This implies that the complete probabilistic description of a random process is the infinite-dimensional PDF. Such an infinite-dimensional joint PDF is difficult to use in practice, as its parameters are difficult to calculate from the real data. [Fenton and Griffiths, 2008]

In order to simplify the problem it is assumed that the random field is a Gaussian and stationary process. In the Gaussian process the joint PDF is a multivariate normally distributed random process. This will lead to the advantage that the complete distribution can be specified by just the mean vector and covariance matrix. In a stationary process the joint PDF is independent of spatial position, implying that the mean, covariance and higher order moments are constant in space (or time), and this results in a point PDF, which is also constant in space. Weak stationarity or second-order stationarity means that only the mean and variance are constant in time. [Fenton and Griffiths, 2008]

So based on these assumptions, a Gaussian and stationary random field requires a constant mean and constant standard deviation.

3.1.1 Correlation Function

The third characteristic of a random field is its correlation function, which is used in order to describe how the field varies in space. The correlation function of a random field $X(x,y)$ is defined as the correlation between two locations which are Δx apart horizontally in the x-direction and Δy apart vertically in the y-direction:

$$\rho(\Delta x,\Delta y) = \rho(X(x,y),X(x+\Delta x,y+\Delta y)) = \frac{Cov(X(x,y),X(x+\Delta x,y+\Delta y))}{\sqrt{Var(X(x,y))}\cdot\sqrt{Var(X(x+\Delta x,y+\Delta y))}} \tag{3.1}$$

where,

Cov	covariance
$Var = \sigma^2$	variance

Since it was assumed that the random field is stationary, the correlation function becomes:

$$\rho(\Delta x,\Delta y) = \frac{Cov(X(x,y),X(x+\Delta x,y+\Delta y))}{Var(X)} \tag{3.2}$$

There are several candidate correlation functions available. For soil properties a commonly applied model is the exponential (Markov) correlation function, in which the correlation decays exponentially with distance. [JCSS-C1, 2006]. As seen in Figure 3.2, in case of a two-dimensional random field this model is given by:

$$\rho(\Delta x,\Delta y) = \exp\left(-\frac{2|\Delta x|}{\delta_x} - \frac{2|\Delta y|}{\delta_y}\right) \tag{3.3}$$

where,

$\Delta x, \Delta y$	distances between points in x and y directions
δ_x, δ_y	correlation lengths or scales of fluctuations in x and y directions

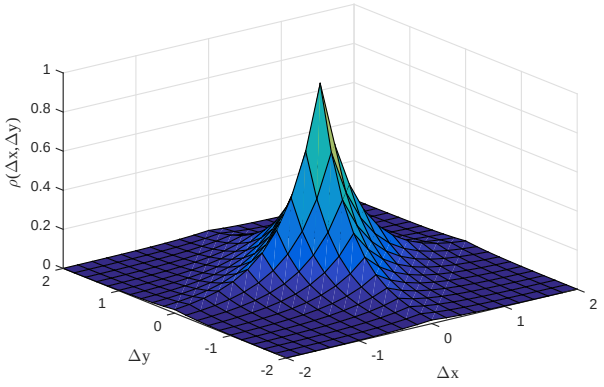

Figure 3.2: Exponential (Markov) correlation function with $\delta_x = \delta_y = 1\,\text{m}$.

For this project, an ellipsoidal Markovian correlation structure is assumed and is expressed as [Sarma et al., 2015]:

$$\rho(\Delta x, \Delta y) = \exp\left(-2\sqrt{\left(\frac{\Delta x}{\delta_x}\right)^2 + \left(\frac{\Delta y}{\delta_y}\right)^2}\right) \tag{3.4}$$

The ellipsoidal Markovian correlation structure forms a quadrant symmetric matrix and develops a properly symmetric well conditioned covariance matrix. Based on this correlation function both isotropic and anisotropic random field can be generated. Isotropy implies that the correlation between two points only depends on the distance between these points and not on their orientation, having equal directional correlation lengths ($\delta_x = \delta_y = \delta$). The isotropic two-dimensional exponential (Markov) correlation function is defined as:

$$\rho(\Delta x, \Delta y) = \exp\left(-\frac{2\sqrt{\Delta x^2 + \Delta y^2}}{\delta}\right) \tag{3.5}$$

On the contrary, an anisotropic random field is generated when the directional correlation lengths differ from each other, which is more common when dealing with soil properties. The effect of correlation length on the correlation structure is illustrated in Figure 3.3.

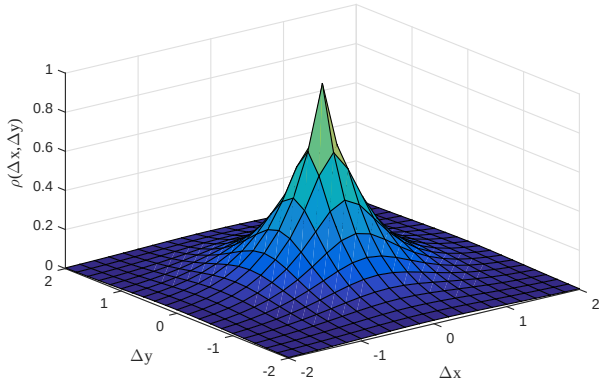

(a)

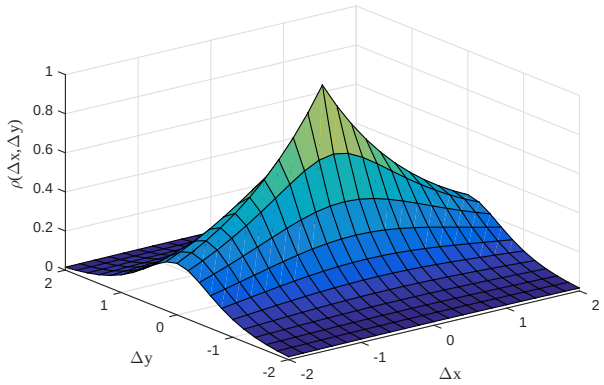

(b)

Figure 3.3: Effect of correlation length on the ellipsoidal Markovian correlation structure: (a) isotropic with $\delta_x = \delta_y = 1\,\text{m}$ and (b) anisotropic with $\delta_x = 3\,\text{m}$ and $\delta_y = 1\,\text{m}$.

3.1.2 Correlation Length

The correlation length or scale of fluctuation is defined as the distance over which properties are significantly correlated, having units of length. This means, that a random field with a large correlation length tend to be more slowly varying and will result in a smoother field. On the other hand, fields having small correlation lengths will vary more irregularly over shorter distances, appearing very rough. In geotechnics, for naturally deposited soils, the horizontal correlation length is generally larger than the vertical one and this amount can be an order of magnitude. This difference can be explained by the sedimentary deposition of soil strata due to geological processes. Figure 3.4 shows typical random field realisations of undrained shear strength with different scale of fluctuations.

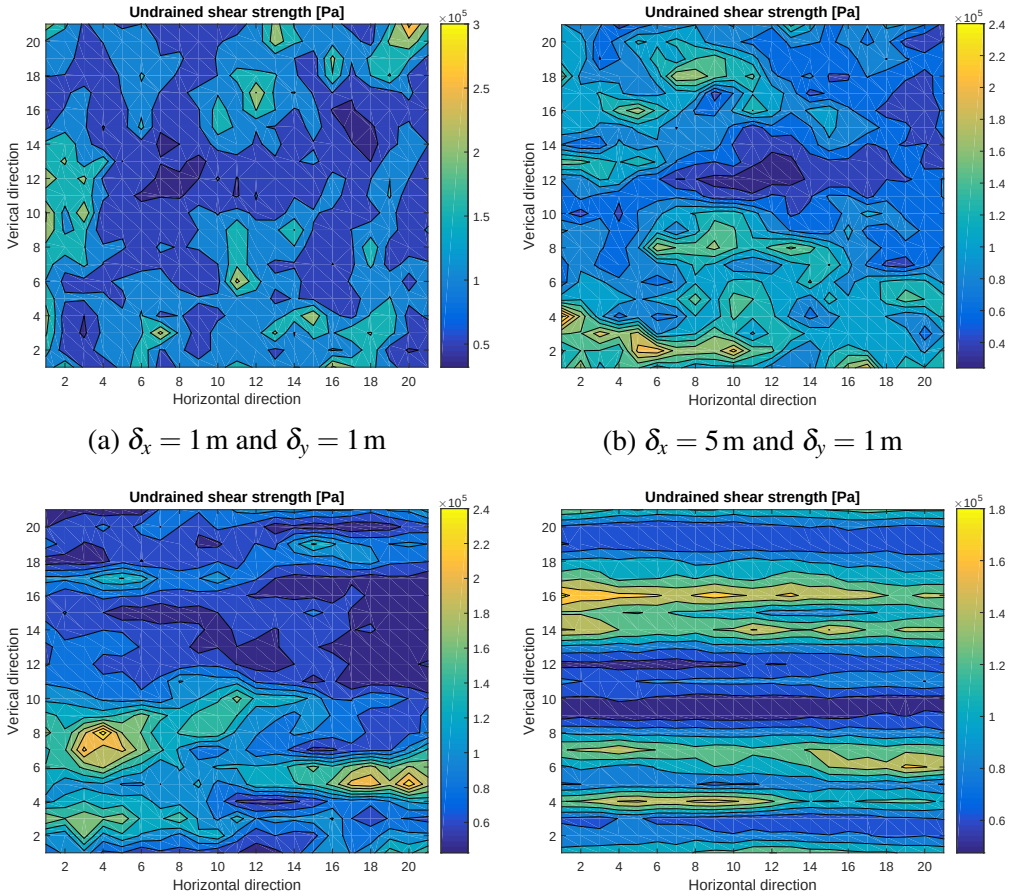

(a) $\delta_x = 1\,\text{m}$ and $\delta_y = 1\,\text{m}$

(b) $\delta_x = 5\,\text{m}$ and $\delta_y = 1\,\text{m}$

(c) $\delta_x = 10\,\text{m}$ and $\delta_y = 1\,\text{m}$

(d) $\delta_x = 100\,\text{m}$ and $\delta_y = 1\,\text{m}$

Figure 3.4: Realizations of the undrained shear strength with different correlation lengths.

It can be seen, that the generated random field highly depends on the chosen correlation length, so care must be taken in choosing these values.

3.1.3 Cross-Correlated Random Fields

When dealing with different random fields, it is important to consider the relationship between them. Different soil properties usually develop a correlation with one another.

In this project the two soil properties are the undrained shear strength and the Young's modulus, and it is assumed that they are cross-correlated. This means that the complete specification of the correlation structure of the two random fields X and Y is characterized by three correlation functions: ρ_X, ρ_Y and ρ_{XY}.

The cross-correlation between X and Y is defined as:

$$\rho_{XY} = \frac{Cov(X,Y)}{\sqrt{Var(X)Var(Y)}} \tag{3.6}$$

For a stationary random field, the cross-correlation reduces to the constant coefficient, ρ, and the correlation between X and Y can be expressed in matrix form as:

$$\rho_{XY} = \begin{bmatrix} 1 & \rho \\ \rho & 1 \end{bmatrix} \tag{3.7}$$

The coefficient of correlation is a relative measure of correlation assuming values between -1 and 1. A value of 0 implies no correlation, a value of -1 indicates full negative correlation in opposite to the value of 1 which will imply a full positive correlation. The coefficient of correlation also measures the closeness of relationship between the two variables X and Y. A positive value implies that X and Y increase together. A negative value will indicate that large values of X are associated with small values of Y. Figure 3.5 shows the cross-correlated random fields, where a full positive correlation is applied. It can be seen that two random fields will have a similar pattern. [DNV, 2012]

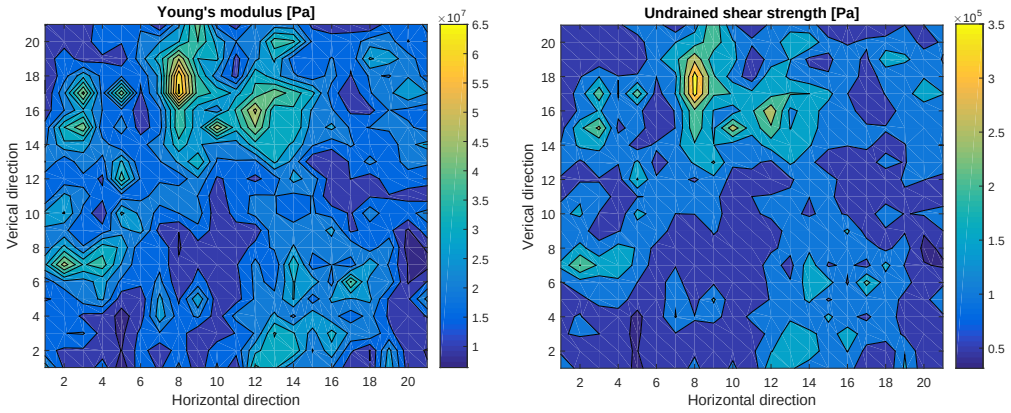

Figure 3.5: Cross-correlated random field for Young's modulus and undrained shear strength with $\rho = 1$.

Figure 3.6 shows that when there is no correlation ($\rho = 0$) the two random fields differ very much.

A complete determination of spatial cross-correlation structure is not likely to happen as this would require a large amount of spatially distributed data. In practice, the complete cross-correlation structure is rarely known. Therefore the cross-corelation between soil properties is defined at a point and estimated by statistically comparing the soil properties in pairs obtained from number of samples assumed to be from the same population. This is defined as pointwise cross-correlation.

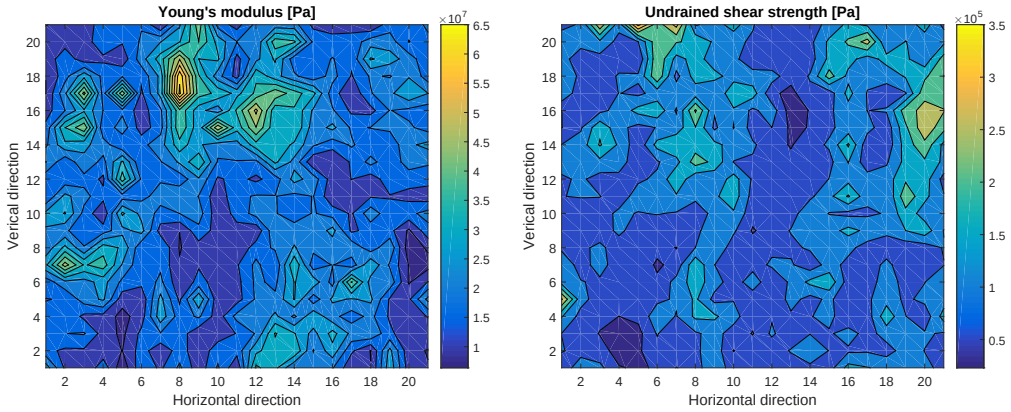

Figure 3.6: Cross-correlated random field for Young's modulus and undrained shear strength with $\rho = 0$.

3.1.4 Probability Distribution

In order to model and describe the distribution of the uncertainties, probability distributions are used. There are different types of distributions available, and therefore it is important to choose the one which fits best with the data. In terms of soil properties the most commonly used are the normal and lognormal distribution. In the following these two types of probability distributions are described.

Normal Distribution

The normal distribution is a distribution model which often is used to represent soil properties. This is largely because sums of random variables tend to a normal distribution. For example, the cohesive strength of a soil is due to the sum of a very large number of electro-chemical interactions taking place at the molecular level - thus, the normal distribution has been widely used to represent the distribution of cohesion. The normal distribution of a random variable X is fully described by its mean value and standard deviation and its probability density function has the following form:

$$f(x) = \frac{1}{\sigma_X \sqrt{2\pi}} \left[-\frac{1}{2} \left(\frac{x - \mu_X}{\sigma_X} \right)^2 \right] \quad \text{for} -\infty < x < \infty \tag{3.8}$$

The normal distribution is symmetric about the mean and can take on negative values. Because soil parameters, such as the undrained shear strength, are nonnegative this might be a disadvantage. For example, when modelling the Young's modulus with normal distribution, there would be a nonzero probability of obtaining a negative Young's modulus. Since a negative elastic modulus does not occur in practice, the normal cannot be its true distribution. This error may be small when the coefficient of variation is small ($COV \leq 0.3$), meaning that the probability of negative values will usually be negligible. If the coefficient of variation is large ($COV > 0.3$), there may be a risk of getting negative outcomes. A simple way to avoid this is to fit a nonnegative distribution. [DNV, 2012], Fenton and Griffiths [2008]

The lognormal distribution cannot reach negative values, as seen on Figure 3.7 and therefore it is a better choice to model the variability of soil parameters.

Lognormal Distribution

The lognormal distribution is defined such that if the variable X is lognormally distributed, then its natural logarithm is normally distributed. If the mean and standard deviation of the random variable are μ_X and σ_X respectively, then the Gaussian field can be transformed to a lognormally distributed field, with the standard deviation and mean given by Eq. (3.9) and Eq. (3.10).

$$\sigma_{\ln X} = \sqrt{\left\{\ln\left[1+(COV_X)^2\right]\right\}} \tag{3.9}$$

$$\mu_{\ln X} = \ln \mu_X - \frac{1}{2}\sigma_{lnX}^2 \tag{3.10}$$

and its probability density function has the following form:

$$f(x) = \frac{1}{x\sigma_{\ln X}\sqrt{2\pi}} \exp\left[-\frac{1}{2}\left(\frac{\ln x - \mu_{\ln X}}{\sigma_{\ln X}}\right)^2\right] \quad \text{for } 0 \leq x < \infty \tag{3.11}$$

As a comparison, the normal and lognormal distribution for the same mean and coefficient of variation is illustrated on Figure 3.7.

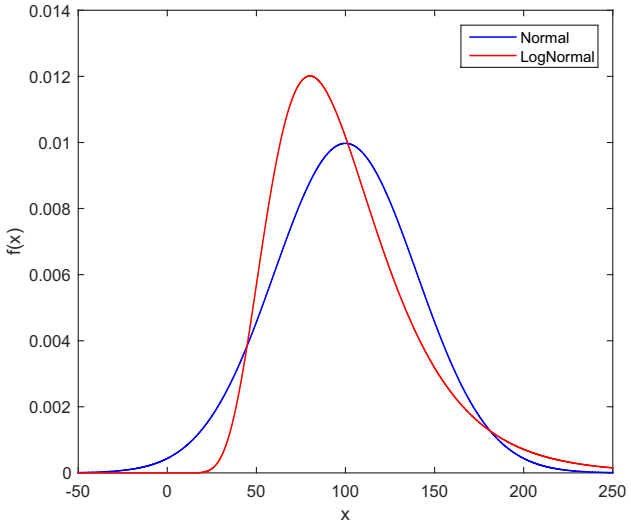

Figure 3.7: Normal and lognormal distribution with μ = 100 kPa and COV = 0.4.

3.2 2D Random Field Generation

This section describes the method used to generate the random fields.

In the present there are several methods available to generate multi-dimensional random fields. Some of the most common ones are stated below [Fenton and Griffiths, 2008]:

- Matrix Decomposition (MD) Method,
- Turning Bands Method (TBM),
- Moving Average (MA) method,
- Local Average Subdivision (LAS) method,
- Fast Fourier Transform (FFT) method,
- Discrete Fourier Transform (DFT) method.

In this project the matrix decomposition method was chosen in order to generate the random fields.

3.2.1 Matrix Decomposition Method

The matrix decomposition (MD) method is simple to implement in practice and it allows fields of irregular geometry without additional computational effort. It is a direct method of generating a random field with the specified correlation function. If the correlation matrix, $\boldsymbol{R}$, is a positive definite matrix then the Cholesky decomposition factorises it into a lower triangular matrix, $\boldsymbol{L}$, and its conjugate transpose, as seen in Equation (3.12) [**?**]:

$$\boldsymbol{R} = \boldsymbol{L}\boldsymbol{L}^T \tag{3.12}$$

The procedure to generate a two-dimensional cross-correlated random field using the matrix decomposition method is described in the following steps [Vahdatirad, 2014]:

1. Assign an index to each discrete point in the field.
2. Construct the distance matrix in x- and y directions.
3. Calculate the correlation matrix, $\boldsymbol{R}$, for the random field, using the specified correlation function in Equation (3.4).
4. Find the lower triangular matrix, $\boldsymbol{L}$, by using Equation (3.12).
5. Based on the cross-correlation matrix, $\boldsymbol{\rho_{XY}}$, defined in Equation (3.7) find the lower triangular matrix, $\boldsymbol{Lcross}$.
6. Generate standard normally distributed random variables, stored in $\boldsymbol{U}$.
7. Apply correlation for each random field by Equation. (3.13):

$$\boldsymbol{G} = \boldsymbol{L} \times \boldsymbol{U} \tag{3.13}$$

8. Apply cross-correlation between the random fields by Equation (3.14)

$$\boldsymbol{Y} = (\boldsymbol{Lcross} \times \boldsymbol{G'}) \tag{3.14}$$

In this project two random fields are generated, one for the uncertainity in the undrained shear strength, $\boldsymbol{Y}_{cu}$, and one in Young's modulus, $\boldsymbol{Y}_E$. These cross-correlated random fields are Gaussian. As it was mentioned earlier, for soil properties a lognormal distribution is a better fit, as it cannot reach negative values. Therefore the standard Gaussian random fields (normal distribution) are transformed into lognormally distributed fields by the following:

$$\boldsymbol{W}_{cu} = \exp\left(\mu_{\ln_{cu}} + \sigma_{\ln_{cu}} \boldsymbol{Y}_{cu}\right) \tag{3.15}$$

$$\boldsymbol{W}_{E} = \exp\left(\mu_{\ln_{E}} + \sigma_{\ln_{E}} \boldsymbol{Y}_{E}\right) \tag{3.16}$$

where,

$\boldsymbol{W}_{cu}$	lognormally distributed random field for undrained shear strength
$\boldsymbol{W}_{E}$	lognormally distributed random field for Young's modulus
$\mu_{\ln_{cu}}$	lognormal mean value for undrained shear strength
$\mu_{\ln_{E}}$	lognormal mean value for Young's modulus
$\sigma_{\ln_{cu}}$	lognormal standard deviation for undrained shear strength
$\sigma_{\ln_{E}}$	lognormal standard deviation for Young's modulus
$\boldsymbol{Y}_{cu}$	normally distributed random field for undrained shear strength
$\boldsymbol{Y}_{E}$	normally distributed random field for Young's modulus

Based on this, two Matlab scripts were written in order to generate two-dimensional random fields. In the first Matlab function, **twoDCrossRandomfield_func.m** the two-dimensional cross-correlated standard normally distributed random fields are generated, depending on the assumptions made. This follows the eight steps described earlier. The second Matlab function, **twoDRandomfield_func.m** transfers the Gaussian random fields into lognormal distributed ones, with uncertainity in the undrained shear strength, and in Young's modulus, as stated in Equation (3.15) and (3.16).

CHAPTER 4

Probabilistic Computational Modelling

A main concern of this project is to model the soil as heterogeneous material. To do this a probabilistic computational model is necessary, in which the concept of random field is used in order to take into account the uncertainties related to soil properties. Modelling the random field is performed using the finite element method, in which the material property in each element is assigned to the generated field's random value. Then, performing Monte Carlo simulation, this method will be repeated so that every time a different random field is generated. The result of this probabilistic computational model will be the probability distribution function of the bearing capacity, for both the footing and embankment. This probability distribution function will be further used as the resistance distribution through a reliability analysis in order to find the probability of failure and based on that to calibrate the factor of safety.

4.1 Probabilistic Finite Element Model

This section describes in detail how the probabilistic finite element (FE) model is created. This was done using different packages:

- Abaqus
- Python scripts
- Fortran subroutines
- Matlab

Abaqus is responsible for running the FE analysis. Python scripts are used to create the FE model, then to submit it to Abaqus and in the end to extract the results from the Abaqus output database (ODB). This allows to change the geometry of the model more easily, which would be time consuming or practically impossible in the graphical user interface (GUI) and on the other hand, as numerous simulations are to be run Python scripting is a good solution to automate this. Fortran subroutines are used to define the soil material model and they are also main tools to map the random fields onto the FE model. Last, Matlab scripts are generating the random fields and they are responsible for managing the whole calculation process. [Vahdatirad, 2014]

The whole procedure of creating and analysing the probobalistic FE model can be divided into three steps. First an FE model is created in order to get the coordinates of the integration points of the elements. This is saved and is ready for further modification. Then the random fields are created, which have the same size as the number of integration points. In this project two random fields were created, one for the undrained shear strength, c_u, and one for the elastic modulus (Young's modulus), E, of the soil. The method for generating these random fields is described in detail in the Section 3.2. In the last step the random fields are mapped as solution-dependent variables (SDVs) in each integration point of the soil elements using a user-defined material subroutine (UMAT). One of the state variables (SDV2) is storing the random field for Young's modulus and the other one (SDV3) stores the undrained shear strength.

As mentioned, Phython scripts are used to construct the FE model and communicate with Abaqus, namely three: **InitialPythonCoords.py**, **InitialPython.py** and **OdbsProcess.py**. These are described in details in the following.

4.1.1 InitialPythonCoords

This Python script is responsible to construct the FE-model without performing any calculations on it. It generates a so-called dummy job in order to extract the coordinates of the integration points of the soil elements. Here the magnitude of the applied load and soil properties are not important. In the script the following main steps are performed:

Geometry

The geometry is generated by using a combination of points, lines which are assemled in the end. All of these points and lines are defined as sets so it is always easy to refer back to them.

Mesh generating

The mesh is generated based on the type of the elements and their size. Mesh refinement along with mesh control can be used here.

Material properties

The different soil materials are created with elasticity parameters. Here dependent variables are also generated, with the purpose to use them as memory space for the stochastic random fields. After this the different materials are assigned to the different sections.

Boundary conditions

The boundary conditions are created, which at the base are restrained in both horizontal and vertical directions, and at the two vertical sides are fixed only in the horizontal direction.

Load

Here an inactivated load is applied in order to complete the calculation. This means that the magnitude of the load is not important, and it will result in an undeformed model.

Creating the job to create the input file

The first step is to create an initial input file for Abaqus. After this the initial input file is modified and connected with FORTRAN subroutine (**InitialSubroutine.for**). The InitialSubroutine initializes the solution-dependent state variables (SDVs). Three state variables are initialized: one for the element number, and two for the coordinates (X and Y). The last step in InitialPythonCoords is running the modified Abaqus input file, to find the element numbers and coordinates of the integration points of the FE model and save it as a txt file (**IntegrationPointsCoords.txt**).

4.1.2 InitialPython

The InitialPython script follows almost the same procedure as the InitialPythonCoords. Here the difference is that, the load is now activated and the Python script is connected to the user-defined material subroutine (UMAT), which is a modified Mohr-Coulomb material model, through the main subroutine (**MainSubroutine.for**). This user-defined material is an elastic-perfectly plastic Mohr-Coulomb material model, in which the material properties can be defined as state variables.

4.1.3 OdbsProcess.py

This script is responsible to extract the specified results at the reference nodes from the Abaqus output database (ODB file).

To summarize it, Figure 4.1 shows the procedure for the probabilistic FE model.

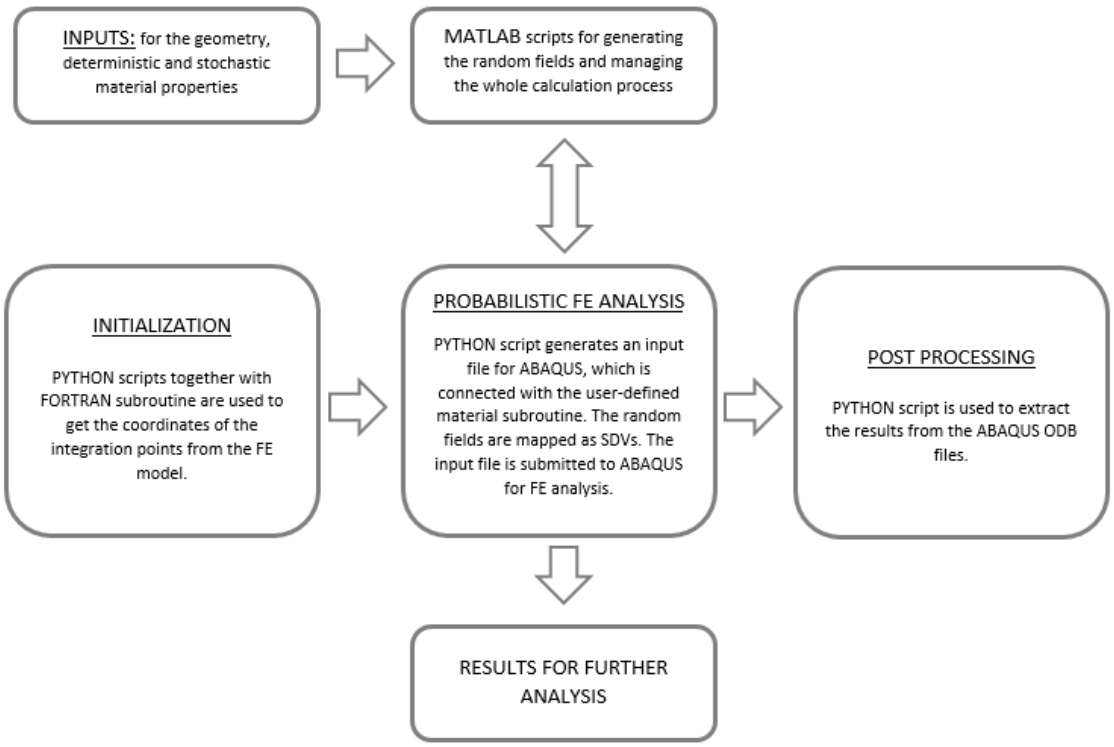

Figure 4.1: Procedure for the probabilistic FE model.[Vahdatirad, 2014]

4.2 Material Model

The material model used to characterize the soil in this project is a user defined material model, which is modified Mohr-Coulomb material model, implemented by Associate Professor Johan Clausen [Clausen et al., 2007].

The Mohr-Coulomb material model used in Abaqus is described in Appendix A. Here an exact form of the Mohr-Coulomb criterion is implemented, but with a different formulation for the plastic flow compared to the one that it is traditionally used. The traditionally employed plastic potential has a six-sided shape, as seen in Figure 4.2.

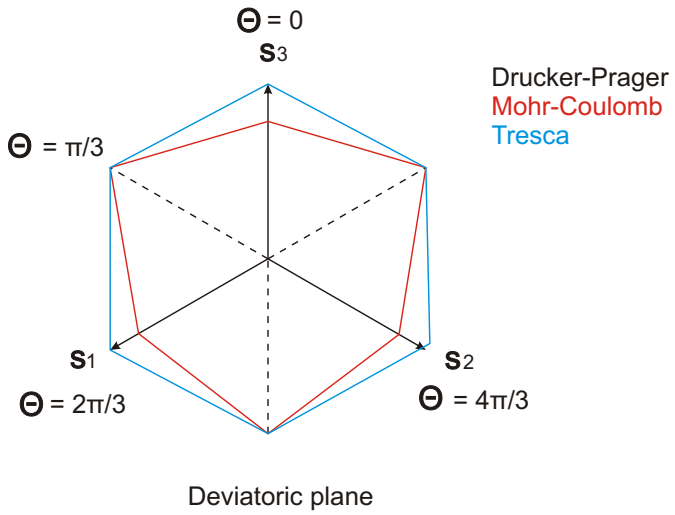

Figure 4.2: Mohr-Coulomb yield surface in the deviatoric plane.

The plastic potential used in Abaqus is rounded in the octahedral plane, and hence the plastic strains will differ from those of the traditional potential. The flow potential used in Abaqus is shown in Figure 4.3.

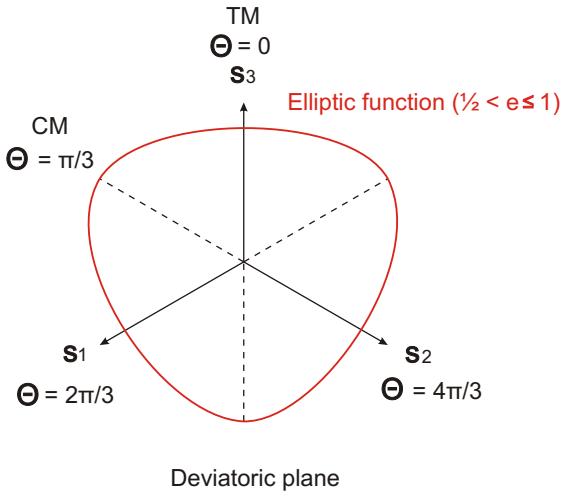

Figure 4.3: Flow potential in the deviatoric plane - Abaqus.

The user defined material model used in this project is based on the traditional Mohr-Coulomb model, where the plastic potential has a six-sided shape, possessing corners and an apex, which causes numerical difficulties. The modification of the material model is based on a transformation into principal stress space and is valid for all linear isotropic plasticity models in which corners and apexes are encountered. [Clausen et al., 2007].

The above described user defined Mohr-Coulomb material assumes linear elasticity and it is described by: Young's modulus, E, Poisson's ratio, μ, cohesion, c, friction angle, ϕ and dilatation angle, ψ.

In this project, both the footing and embankment involve undrained clay as soil material, satisfying the Tresca failure criterion, as seen in Figure 4.2, in which the friction and dilatation angle is assumed to be 0. It should be noted that in the user defined material model these parameters cannot be set to 0, therefore these take the value of 0.00001.

4.3 Finite Mesh

It is important to discretize the problem in a way which is closest to the reality. Therefore, the element type which is used in the finite element model plays an important role, and it should be chosen carefully. In order to analyse the problem the finite element mesh uses a two-dimensional model assuming plain strain and it is discretized into a number of 8-node bi-quadratic, reduced integration, hybrid elements (CPE8RH). The need for this type of elements is described in the following.

For undrained soil conditions it is an appropriate assumption that the material exhibits a nearly-incompressible behaviour. This type of behaviour can be characterized with a bulk modulus, K very much larger than the shear modulus, G, or in other words when the Poisson's ratio, μ is greater than 0.48. In a near-incompressible behaviour a very small change in displacement produces extremely large changes in pressure. Therefore, the solution cannot be obtained in terms of the displacement history only, since a purely hydrostatic pressure can be added without changing the displacements. Abaqus [2013]

A nearly-incompressible material response cannot be modelled with regular elements because the pressure stress in the element is indeterminate. This is not the case in the hybrid element, where the pressure stress is treated as a basic solution variable coupled to the displacement variable to approximate the equilibrium equations and compatibility conditions.

For an incompressible material each integration point's volume must remain almost constant. This overconstrains the kinematically admissible displacement field and causes volumetric locking. Due to this, finite element meshes often exhibit overly stiff behaviour, as seen in Figure 4.4.

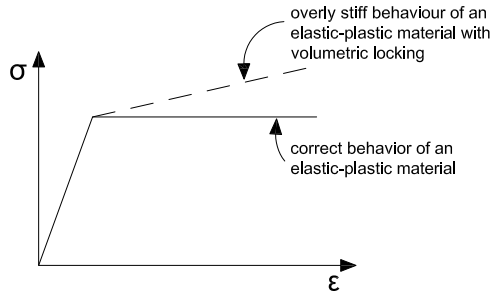

Figure 4.4: Effect of volumetric locking.[ESC]

In order to eliminate the volumetric locking, reduced integration is used. This means that the number of integration points will be reduced as seen in Figure 4.5 and 4.6. The 8-noded element with full integration has nine integration points, but this will be reduced to 4 when reduced integration is applied.

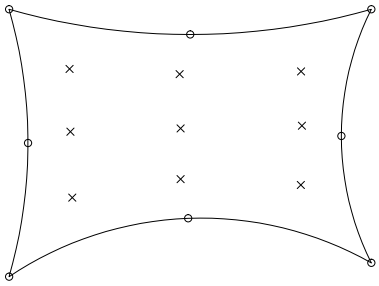

Figure 4.5: 8-node full integration element.

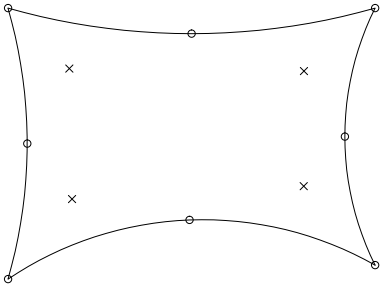

Figure 4.6: 8-node reduced integration element.

Another type of element, 6-node modified, with hourglass control, hybrid with linear pressure (CPE6MH) was also used in this project. This was only used as a part of the convergence analysis, and it showed that it is less efficient than CPE8RH elements. Figure 4.7 shows the nodes and integration points of this element type.

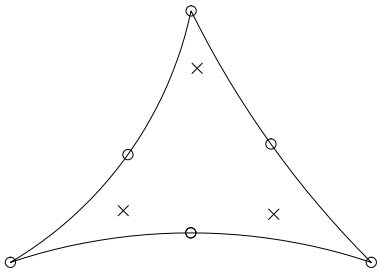

Figure 4.7: CPE6MH element.

4.4 Numerical Method

When modelling the soil at high loads a number of non-linearities can be discovered, which means that Hooke's law becomes invalid, resulting in a non-linear stress-strain relation. Therefore the elasto-plastic relations in the finite element method are implemented in two different levels: global and material level. In order to calculate the strain increments an equilibrium at the global level needs to be reached. In order to satisfy the equilibrium condition, global iterative procedures are applied. On the material level, the plasticity relations must be satisfied, and the stress increments are calculated by integration of the stress rates.

Abaqus uses the Newton-Raphson method to obtain solutions for non-linear problems. Here the solution is found by applying the specified loads gradually and incrementally working toward the final solution. Therefore, Abaqus breaks the simulation into a number of load increments and finds the approximate equilibrium configuration at the end of each load increment. It often takes Abaqus several iterations to determine an acceptable solution to a given load increment. The sum of all of the incremental responses is the approximate solution for the non-linear analysis. **??**

The non-linear response of a structure to a small load increment, Δf , is shown in Figure 4.8. In the elasto-plastic analysis this load increment will produce a displacement increment, Δu. The incremental relation between the displacement and force is the following:

$$[K_t]\{\Delta u\} = \{\Delta f\} \tag{4.1}$$

$[K_t]$	tangent stiffness matrix
$\{\Delta u\}$	displacement increment vector
$\{\Delta f\}$	load increment vector

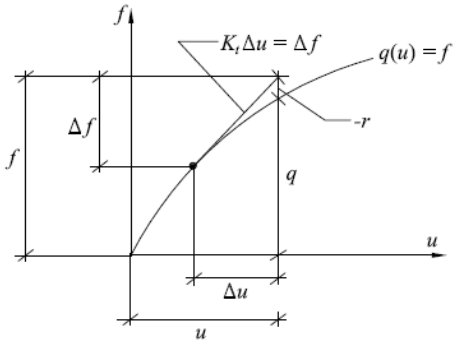

Figure 4.8: Load increment in elasto-plastic computation.[Krabbenhøft, 2002]

Based on Figure 4.8, Abaqus calculates the structure's internal forces. The difference between the total applied load and internal load can be calculated as:

$$\{r\} = \{f\} - \{q\} \tag{4.2}$$

where,

$\{r\}$	residual vector
$\{f\}$	applied force vector
$\{q\}$	internal force vector

Based on Figure 4.8 equilibrium is reached when:

$$\|\{r\}\| < \varepsilon \|\{f\}\| \tag{4.3}$$

During the simulations, the FE analysis of the embankment with a maximum number of increments set to 1000 resulted in a very long computational time sometimes. This long computational time is due to fact that equilibrium is still reached even at an increment number up to 650 where the load step is updated every time. It was noticed that this change in the load step after a certain number of increments becomes negligible. This is illustrated in an example.

Figure 4.9 shows the deformed mesh of the embankment at the 15th increment with a load step (step time) of 0.3387. Next, Figure 4.10 shows the same analysis, but this time at the final increment (658) with a load step of 0.3401. This change is 0.4%, or in other words 99.6% of the bearing capacity is already reached after 15 increments. Therefore, the maximum number of increments will be reduced to a 100, which is a reasonable approach, as it reduces the computational time significantly.

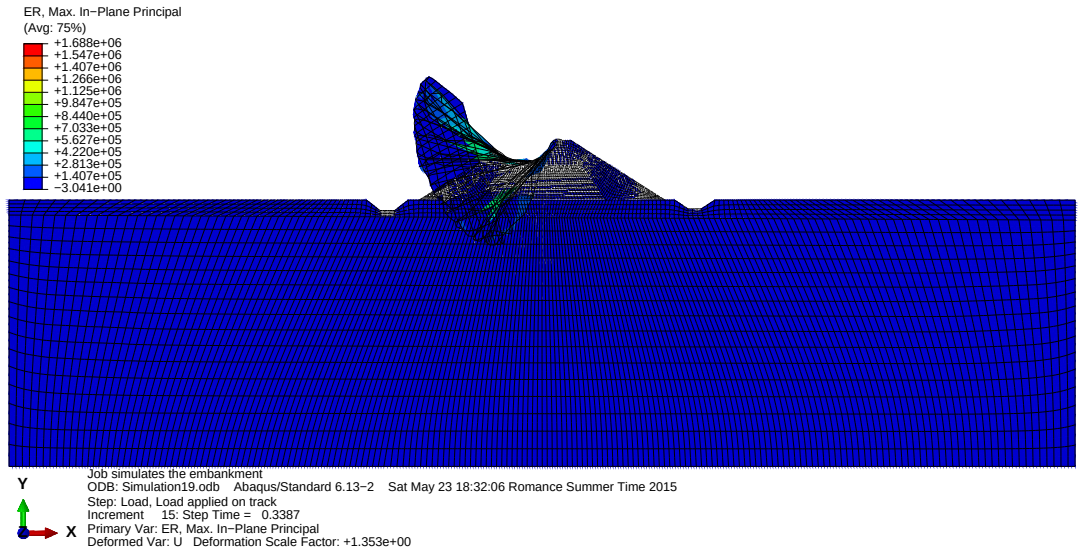

Figure 4.9: Increment: 15.

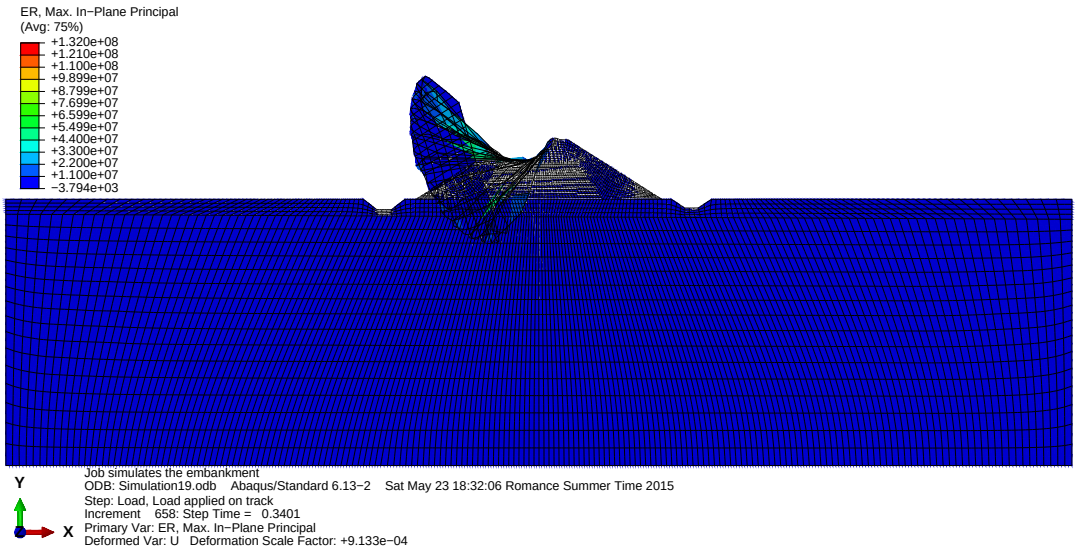

Figure 4.10: Increment: 658.

This approach is used in both of the footing and embankment problem. But it should be emphasised that the results might be slightly different if there was infinite time to do the calculations.

4.5 Modelling of the Load

In this project the load on the structure, both in the case of footing and embankment, is assumed to be a variable action, for example snow or wind, with a Gumbel distribution, as suggested by DS/INF 172 [2009]. Here it is also recommended that for this type of action to use a coefficient of variation, *COV* of 40% and a a 98% quantile characteristic value for a 1 year return period. In the following the Gumbel distribution will be characterized. The load is assumed to be uniformly distributed in a vertical direction.

Gumbel Distribution

The Gumbel distribution is used to model the distribution of the maximum (or the minimum) of a number of samples of various distribution. The normal distribution of a random variable X is fully described by its mean value and standard deviation, as seen on Figure 4.11, and its probability density function has the following form:

$$f(x) = \alpha \exp[-\alpha(x-\beta)] \exp[-\exp[-\alpha(x-\beta)]] \quad \text{for} -\infty < x < \infty \tag{4.4}$$

Here α and β are shape and scale parameters and are related to the mean, μ, and standard deviation, σ, by:

$$\mu = \beta + \frac{0.5772}{\alpha} \tag{4.5}$$

$$\sigma = \frac{\pi}{\alpha\sqrt{6}} \tag{4.6}$$

The cumulative distribution function for a Gumbel distribution is defined as:

$$F_X(x) = \exp[-\exp[-\alpha(x-\beta)]] \tag{4.7}$$

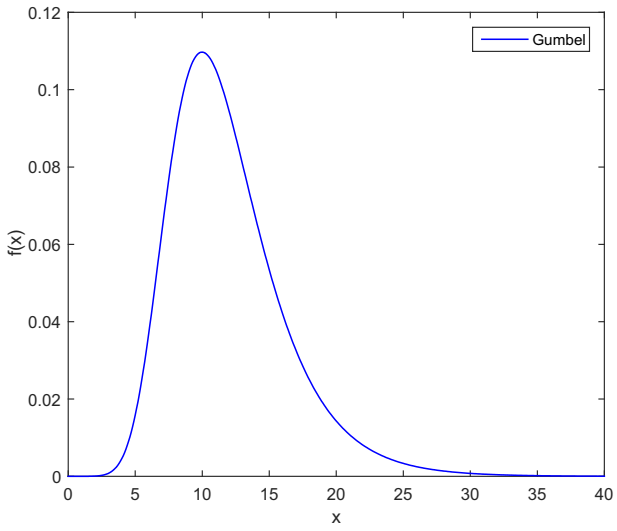

Figure 4.11: Gumbel distribution with μ=11.92 and σ=4.3.

With the distribution type chosen for the load, the next step is to calculate the characteristic value of the load, F_k, which is suggested as a 98% quantile. The quantile, $x_{0.98}$ is defined as $F_X(x_{0.98}) = 0.98$ becomes:

$$x_{0.98} = \beta - \frac{1}{\alpha}\ln(-\ln(0.98)) \tag{4.8}$$

Equation (4.8) written in terms of mean value and coefficient of variation becomes the following:

$$F_k = \mu_F \left(1 - COV_F \frac{\sqrt{6}}{\pi}\left(0.5772 + \ln\left(\ln\left(0.98\right)\right)\right)\right) \tag{4.9}$$

The characteristic value of the load by using Equation (4.8) is for a 1 year return period. From this the return period for the design load can be calculated by the following, which in this case corresponds to a 50 year return period.

$$R = \frac{\tau}{1 - F_X(x_R)} \tag{4.10}$$

where,

τ	time interval between observation (1 year)
$F_X(x)$	distribution for 1 year extremes

4.6 Summary

In the probabilistic approach the uncertainties related to the strength parameters and the load were modelled, through stochastic variables, which are characterized by their mean value, standard deviation and distribution type. The correlation lengths needed to generate the random fields should be carefully chosen, as this influences the failure mechanism of the structure, thus the reliability.

The stochastic model used for the calibration of partial safety factor is shown in Table 4.1.

Table 4.1: Stochastic model.

Variable	Coefficient of variation	Distribution type	Quantile/Confidence
Load (variable)	40%	Gumbel	98% quantile
Undrained shear strength	40%	LogNormal	95% confidence

CHAPTER 5

Reliability Analysis

Reliability analysis is an important tool for quantifying uncertainties in analysis and design of engineering systems. Traditionally structural analysis and design has been based on deterministic methods, where characteristic values of the uncertain loads and resistances are specified and partial safety factors are applied to the loads and strengths in order to ensure that the structure is safe enough. The partial safety factors are usually based on experience or calibrated to existing codes or to measures of the reliability obtained by probabilistic techniques. However, there are a number of situations where probabilistic methods are more efficient in order to deal with the uncertainties related to the loads, strengths and modelling of the system.

A structure is usually required to perform its intended function for a specific period of time under a given set of conditions i.e. it is required that it does not collapse or becomes unsafe and that it fulfills certain functional requirements. The reliability of a structure can be defined as the probability that unsatisfactory performance or failure will not occur. Reliability methods are used to estimate the probability of failure. In this chapter different reliability methods are discussed and based on them the probability of failure, P_f, and the reliability index, β, of the structure are calculated. These numbers will tell us about the safety of the structure and depending on them the partial safety factors are then calibrated.

In general, the probability of failure, P_f, can be presented using the interaction between the load, P, and resistance, R, as seen in Figure 5.1. P and R are modelled by independent stochastic variables with probability density functions f_R and f_S and cumulative distribution functions F_P and F_R. The probability of failure can be calculated as [Sørensen, 2011]:

$$P_f = P(R \leq P) = P(R - P \leq 0) = \int_{-\infty}^{\infty} F_R(x) f_P(x) dx \tag{5.1}$$

In simple terms, the probability of failure can be estimated by the degree of overlap between the distributions, as seen on Figure 5.1. This depends essentially on the separation between the means of the distributions and the spread in each distribution. The area of overlap, P_f, decreases with increasing separation between μ_R and μ_P while P_f increases with increasing spread (σ_R or σ_P) in either distribution. [Sørensen, 2011]

It is noted that it is important that the lower part of the distribution for the strength and the upper part of the distribution for the load are modeled as accurate as possible.

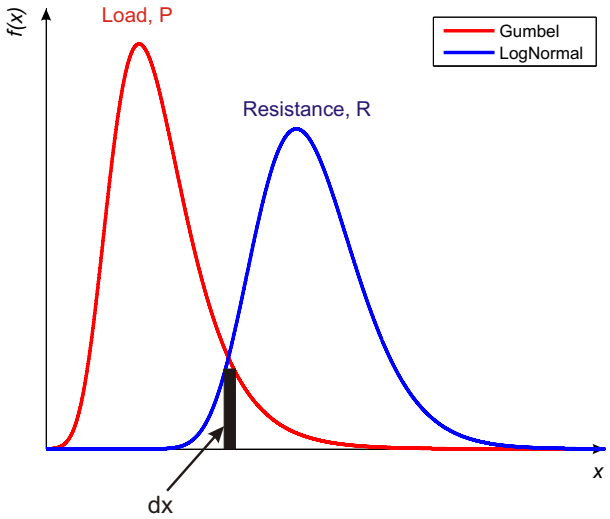

Figure 5.1: Illustration of probability of failure; interaction between loading and resistance effects.

There are many methods that can be used to measure the reliability of a structure. Among them are the first order reliability method (FORM), second order reliability method (SORM) and simulation techniques. In FORM the limit state function (failure function) is linearized compared to SORM, where a quadratic approximation to the failure function is determined. In both of these methods the reliability index is found by performing an optimization process, normally by taking the derivatives of the limit state function with respect to the variables. [Sørensen, 2011]

Figure 5.2 illustrates the difference between the first- and second order reliability methods in u-space. Here it can be seen that the approximation of the failure surface by FORM is a straight line (linear approximation) and the one by SORM is a curved line (quadratic approximation).

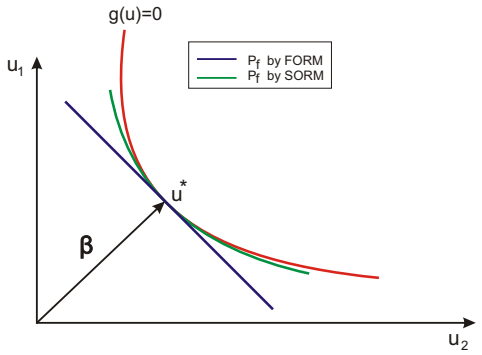

Figure 5.2: Illustration of first and second order approximations of the failure surface. Sørensen [2011]

FORM and SORM come with the disadvantage that in order to make the optimization problem easy to control the number of random variables of the target problem cannot be

too many. As this project deals with geotechnical problems, that include a vast amount of random variables, these methods may not be the best choice. On the other hand FORM is expected to give reasonable results when the failure functions are not too non-linear.

To overcome these limitations it is recommended to use simulation techniques, in which samples of the stochastic variables are generated and the relative number of samples corresponding to failure is used to estimate the probability of failure. The most famous simulation technique is crude Monte Carlo simulation.

5.1 Crude Monte Carlo Simulation

When applying FORM, SORM or simulation techniques it is required that it is possible for given realizations, $\mathbf{x}$, of the basic variables to state whether the structure is in a safe state or in a failure state. Therefore the basic variable space can be divided into sets, the safe set, ω_s and failure set, ω_f, by the failure surface (limit state surface) such as:

$$g(\mathbf{x}) \begin{cases} > 0 & ,\mathbf{x} \in \omega_s \\ \leq 0 & ,\mathbf{x} \in \omega_f \end{cases}$$

Here $g(\mathbf{x})$ denotes the failure function and it is defined as the load bearing capacity or resistance, R, minus the loading, P. This formulation is called the limit state equation.

$$g(\mathbf{x}) = R - P \tag{5.2}$$

where,

$g(\mathbf{x})$	failure function
R	bearing capacity
P	load

The crude Monte Carlo simulation technique involves generating a large number of realisations of the basic random variables and checking whether failure occurred or not for each set of random sample values. This process is repeated several times and the ratio of the number of failures to the total number of simulations gives an estimate of the probability of failure, as defined in Equation (5.3).Sørensen [2011]

$$\hat{P}_f = \frac{1}{N} \sum_{j=1}^{N} I\left[g\left(\hat{\mathbf{x}}_j\right)\right] \tag{5.3}$$

where,

N	number of simulations
$I\left[g\left(\mathbf{x}\right)\right]$	indicator function
$\hat{\mathbf{x}}_j$	sample no. j of a standard normally distributed stochastic vector $\mathbf{X}$

The indicator function is defined by:

$$I\left[g\left(\mathbf{x}\right)\right] = \begin{cases} 0 & \text{if} \quad g(\mathbf{x}) > 0 \quad \text{(safe)} \\ 1 & \text{if} \quad g(\mathbf{x}) \leq 0 \quad \text{(failure)} \end{cases}$$

The simulation is in principle simple and can be performed in two steps. First, in order to simulate outcomes of stochastic variables with an arbitrary distribution, a "pseudo random" number between 0 and 1 is generated for each of the components in $\hat{\mathbf{x}}_j$. In the second step the outcomes of the "pseudo random" numbers z_{ji} are transformed to outcomes of $\hat{x}_{ji}$ by Equation (5.4) as shown in Figure 5.3:

$$\hat{x}_{ji} = F_X^{-1}(z_{ji}) \tag{5.4}$$

where,

F_X^{-1} | cumulative distribution function for random variable, X_i

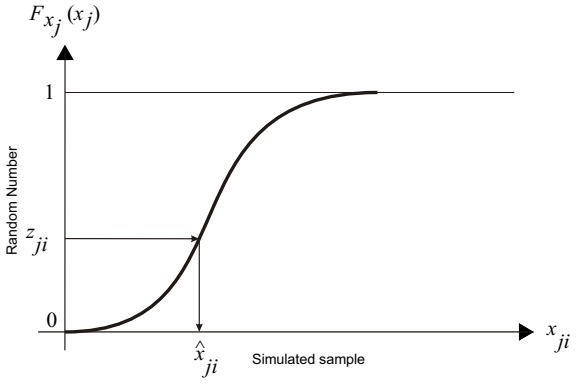

Figure 5.3: Principle for simulation of a random variable.[Sørensen, 2011]

This process is then repeated until all components of the vector $\hat{x}_j$ have been generated.

The required number of simulations can be estimated from:

$$N = \frac{1}{P_f} \tag{5.5}$$

This means that in order to estimate a probability failure of a magnitude of 10^{-5} it is expected that approximately 1 millions simulations are necessary.

In order to measure the statistical accuracy of the estimated probability of failure its coefficient of variation, $COV\,(P_f)$ is calculated by Equation (5.6). [Ayyub and McCuen, 2011]

$$COV\,(P_f) \approx \frac{\sqrt{\frac{P_f\left(1-P_f\right)}{N}}}{P_f} \tag{5.6}$$

It is logical to see that if the number of samples, N approaches infinity the coefficient of variation of the estimated probability of failure, $COV\,(P_f)$ approaches 0.

In order to illustrate the convergence of the simulation process the number of simulation cycles, N, was varied. The results are shown in Figure 5.4 using a non-arithmetic scale for the number of simulations to show the effect of N on P_f and $COV(P_f)$, at small as well as large values.

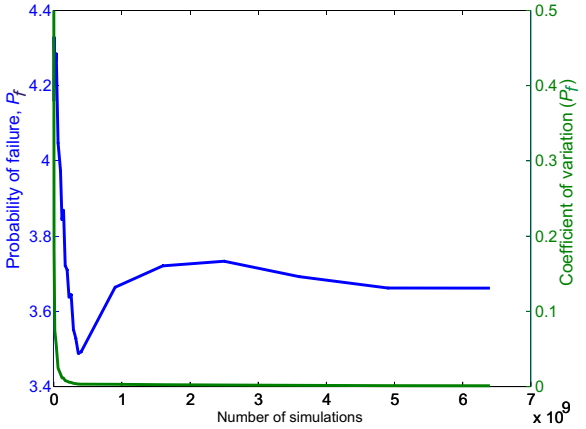

Figure 5.4: Convergence analysis for the crude Monte Carlo simulation - embankment.

It can be observed that a convergence is reached at $N = 5 \cdot 10^9$. As the computational time was short $N = 10^{10}$ simulations are performed in both examples. It should be noted here that this number corresponds for $g(\mathbf{x})$, so 10^5 for R and P, based on Equation (5.2).

A typical realization of the crude Monte Carlo simulation of the resistance, R, and load, P, is illustrated on Figure 5.5.

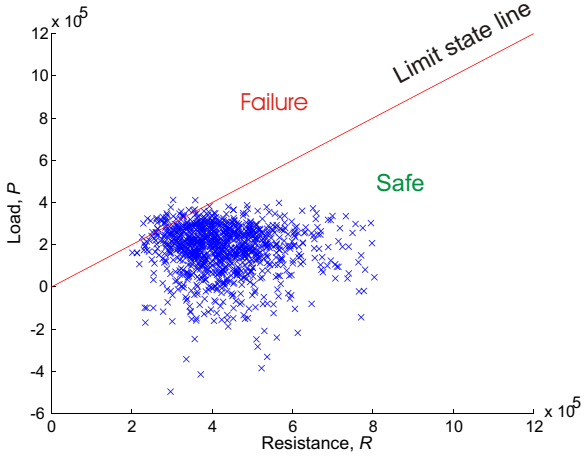

Figure 5.5: Crude Monte Carlo simulation method.

Now that the probability of failure is calculated the reliability index is defined by:

$$\beta = \Phi^{-1}(-P_f) \tag{5.7}$$

where,

Φ | standard normal distribution function

5.2 Calibration of the Partial Safety Factor

The calibration of partial safety factors is performed in such a way that the reliability calculated with the crude Monte Carlo simulation method with the new calibrated partial safety factors is as close as possible to the target reliability index. Therefore, in order to calibrate the partial safety factor of the undrained shear strength, first the target reliability index, β_T should be considered. Table 5.1 shows the proposed target reliabilities and the corresponding annual probability of failures.

Table 5.1: Target reliabilities.

Structure	Target reliability index, β_T	Annual probability of failure, P_f
Footing	3.7	10^{-4}
Embankment	4.7	10^{-6}

The target reliability of 4.7 for the embankment is proposed by the Danish National Annex to DS/EN 1990 [2010] and by Banedanmark [2010]. On the other hand, the footing is assumed to have a low consequence class (CC1) for which DS/EN 1990 [2010] recommends a lower reliability index, 3.7.

The current partial safety factors for the undrained shear strength and load, as defined in the Danish National Annex to DS/EN 1997-1 [2007], are listed in Table 5.2.

Table 5.2: Partial safety factors used in the deterministic calculations.

Parameter	Symbol	Value
Partial safety factor for the undrained shear strength	γ_{cu}	1.8
Partial safety factor for the load	γ_F	1.5

The design value of the undrained shear strength and the load is calculated by Equation (5.8) and (5.9).

$$c_{ud} = \frac{c_{uk}}{\gamma_{cu}} \tag{5.8}$$

$$F_d = F_k \gamma_F \tag{5.9}$$

5.2.1 Deterministic Approach

Usually, in a deterministic design, the necessary dimensions of the structure are calculated based on the design load. After the calculations the dimensions are increased or decreased, depending on the reached bearing capacity. In this project this is done the other way around, meaning that the dimensions of the structures are fixed, and the design load is determined from the FE analysis with a uniform soil, characterized by the design undrained shear strength, calculated by (5.8). The design load is calculated as 99% of the resistance as seen in Equation (5.10)

$$F_d = 0.99R_d \tag{5.10}$$

where,

R_d | resistance from the deterministic FE analysis

The assumption of the design load being 99% of the resistance was done in order to take into consideration the possibility of a not full convergence and the approach used regarding the number of increments, presented in Section 4.4, where the maximum number of increments was lowered down to a 100.

5.2.2 Workflow

In the following, the calculations steps used in this project, in order to calibrate the partial safety factor are described:

1. The design load, F_d, is determined from a deterministic calculation with uniform soil, having the same undrained shear strength, c_{ud}, in all points of the model
2. The characteristic value of the undrained shear strength, c_{uk}, is:

$$c_{uk} = c_{ud}\gamma_{cu} \tag{5.11}$$

3. Now with the known characteristic value with 95% confidence level for the mean strength, and based on Schneider's equation the mean value is found as:

$$\mu_{cu} = \frac{c_{uk}}{1 - 0.5COV_{cu}} \tag{5.12}$$

4. In order to model the uncertainties in c_u and E cross-correlated random fields are generated, having LogNormal distribution, based on the known mean value, coefficient of variation, correlation lengths and covariance matrix.
5. A number of Monte Carlo (MC) simulations are performed to determine the bearing capacity of the structure in ULS, resulting in a catalogue of bearing capacities. A well-suited probability distribution function is fit to the data.
6. The characteristic load, F_k, is found as:

$$F_k = \frac{F_d}{\gamma_F} \tag{5.13}$$

7. Based on the coefficient of variation and probability distribution of the load, and on the fact that the characteristic value of the load is a 98% quantile, the mean value, μ_F, is found and then, subsequently:

$$\sigma_F = \mu_F COV_F \tag{5.14}$$

8. Based on the probability density function of the load combined with the probability density function of the resistance, it is possible to make a number of realizations, performed with the crude Monte Carlo simulation technique.

9. From all the realisations the yearly probability of failure and reliability index is calculated.

10. If this probability of failure is too low, this means that the partial safety factor of the undrained shear strength is too high, and vice versa. The partial safety factor is then calibrated until the target reliability index is reached. It should be noted here that the partial safety factor for the load remains fixed through the calculations.

Part II

Practice

CHAPTER 6

Footing

One of the fundamental geotechnical problems is the bearing capacity of a strip footing. In this chapter a probabilistic analysis of the bearing capacity of a strip footing is performed together with a reliability analysis, through which the partial safety factor for the strength of the soil is calibrated, based on the workflow described in Section 5.2. The soil is assumed to be clay and the analysis is performed assuming undrained conditions satisfying the Tresca failure criterion (friction angle, φ is set to 0). Analytical calculations are also performed, which gives an idea about, what the bearing capacity is.

6.1 Problem Definition

In the following, the problem definition and the finite element model is discussed. The footing with a width of B = 2m is lying on linearly elastic - perfectly plastic Mohr-Coulomb soil. The footing is lying on the ground surface, meaning that the surcharge load, q is equal to 0. The geometry of the surface footing problem is shown in Figure 6.1.

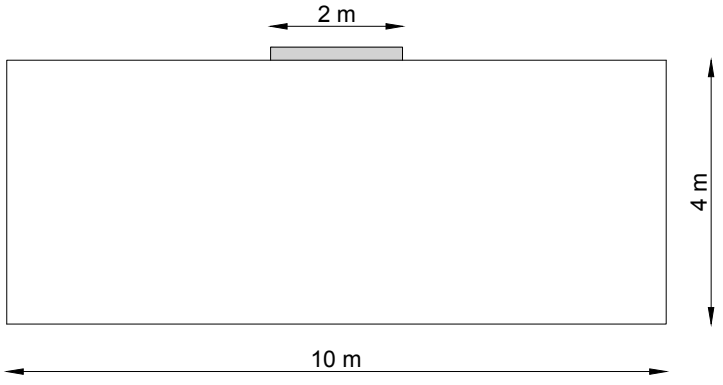

Figure 6.1: The geometry of the footing problem.

The size of the finite element model is 10.0 m by 4.0 m, and it is large enough to keep the boundary conditions at the bottom and the right side from restricting the soil movement due to the footing load, as deformations may still occur at a large distance from the action, especially for undrained analysis.

In order to analyse this problem the finite element mesh uses a two-dimensional model assuming plain strain. The calculations are carried out for a rough footing, which means that at the base of the footing no displacements are allowed in the x direction. The boundary conditions at the base are restrained in both horizontal and vertical directions, and at the two vertical sides are fixed only in the horizontal direction.

The characteristic value of the undrained shear strength is presented in Table 6.1.

Table 6.1: Characteristic value of the undrained shear strength for the footing.

Parameter	Value
c_{uk} [kPa]	108

The footing itself is modelled as an material with very high stiffness, assuming a very large Young's modulus.

6.2 Analytical Calculations

In the following the analytical approach to calculate the bearing capacity of a strip footing is presented. In this way the FE model can be validated. The analytical calculations are based on Terzaghi's bearing capacity formula.

The Terzaghi formulation for determination of the ultimate bearing capacity of shallow rough rigid continuous (strip) foundations supported by a homogeneous soil layer is shown in Equation (6.1).

$$q_u = cN_c + qN_q + \frac{1}{2}\gamma BN_\gamma \tag{6.1}$$

where,

c	cohesion of soil
q	overburden pressure at the bottom of the foundation
γ	unit weight of soil
B	width of foundation
N_c, N_q, N_γ	bearing capacity factors

The failure mechanism assumed by Terzaghi for determining the ultimate bearing capacity for a rough strip footing located at a depth, D_f, measured from the ground surface is shown in Figure 6.2.

As it is assumed that the footing in question is a surface footing lying on undrained clay, the term describing the overburden pressure and the term including the unit weight of the soil can be excluded.

The bearing capacity for the strip footing on clay becomes:

$$q_{u_{Terzaghi}} = c_u(2+\pi) \tag{6.2}$$

With an undrained shear strength, c_{ud}, of 60 kPa, the bearing capacity is:

$$q_{\mathrm{u_{Terzaghi}}} = 308.4\,\mathrm{kPa}$$

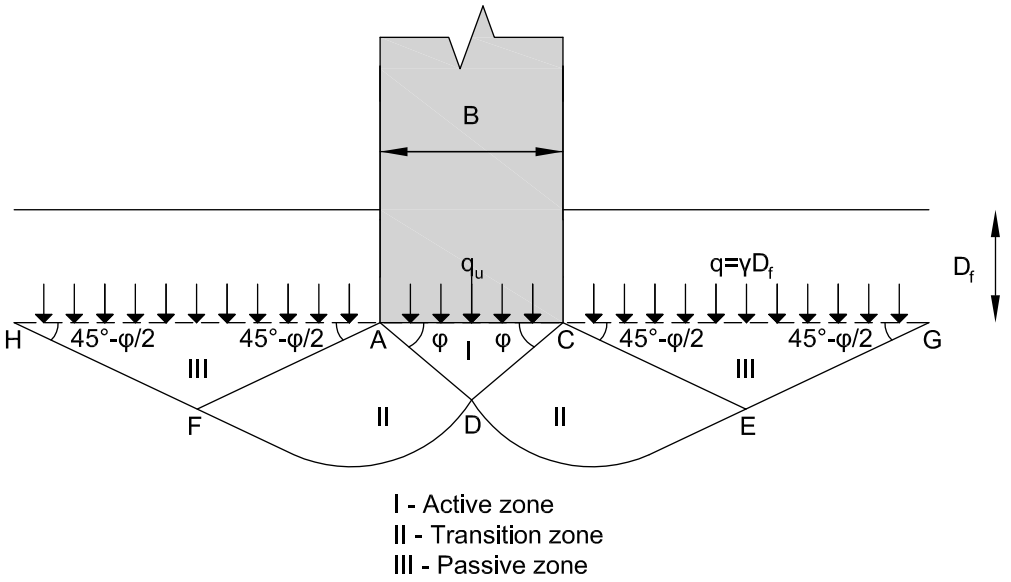

Figure 6.2: Terzaghi's theory for bearing capacity of strip footing. [Azizi, 2000]

6.3 Convergence Analysis

In order to be sure that the chosen topology and element type will lead to correct results a convergence analysis has been carried out for the bearing capacity of the strip footing in clay, and it is shown in Figure 6.3. This includes two element types CPE8RH and CPE6MH, respectively. It should be noted that in the convergence analysis the random fields are not applied, so that a homogeneous soil is investigated.

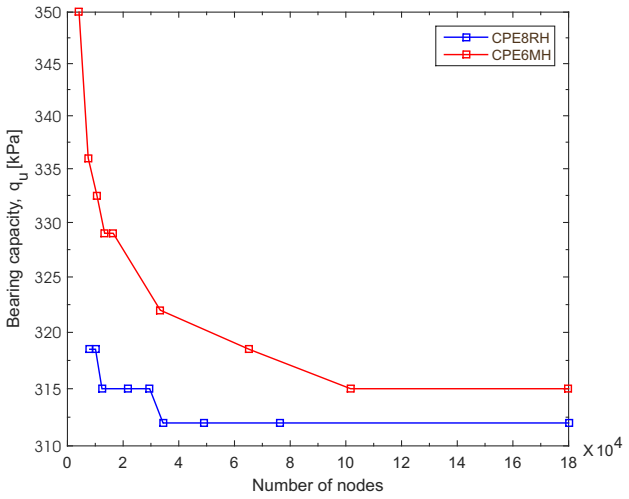

Figure 6.3: Convergence analysis of bearing capacity.

Figure 6.3 shows that the CPE8RH elements have better convergence, and they already converge at 12405 nodes which corresponds to 4040 elements. On the other hand this element type is better, because it results in a bearing capacity which is a lot closer to the analytical solution and it needs less computational time. Based on this, the FE simulations and deterministic calculations for the strip footing will be performed with a finite mesh consisting of 4040 elements.

6.4 Deterministic Calculations

The design load is determined from the FE analysis with a uniform soil having an undrained shear strength, c_{ud}, of 60 kPa ($\gamma_{cu} = 1.8$). The analysis resulted in a bearing capacity, q_u, equal to 316 kPa, which is shown on the load-displacement curve on Figure 6.4. Based on this, the design load for the footing is found as 99% of the bearing capacity:

$$F_d = 313\,\text{kPa}$$

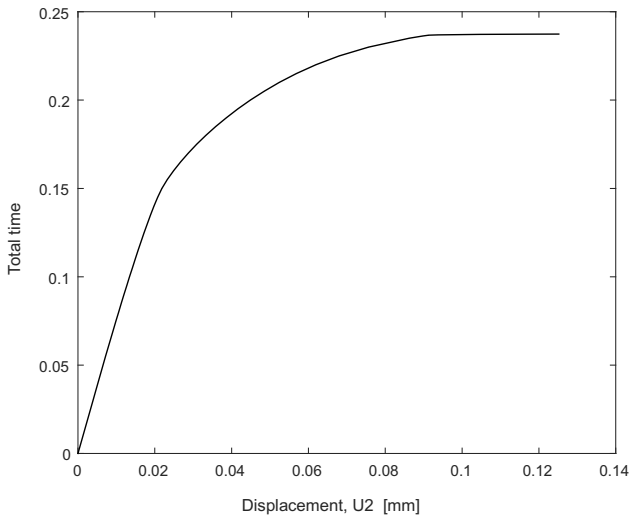

Figure 6.4: Load-displacement curve - deterministic calculation.

Further calculations were performed with different design values, corresponding to different partial safety factors. It was found, as seen in Figure 6.5, that there is a linear relationship between the undrained shear strength, c_{ud}, and the resistance, R_d. This way, there is no need to perform the deterministic calculations each time when the partial safety factor is being calibrated. Instead the linear relation between them is used, so the resistance can be calculated and subsequently the design load.

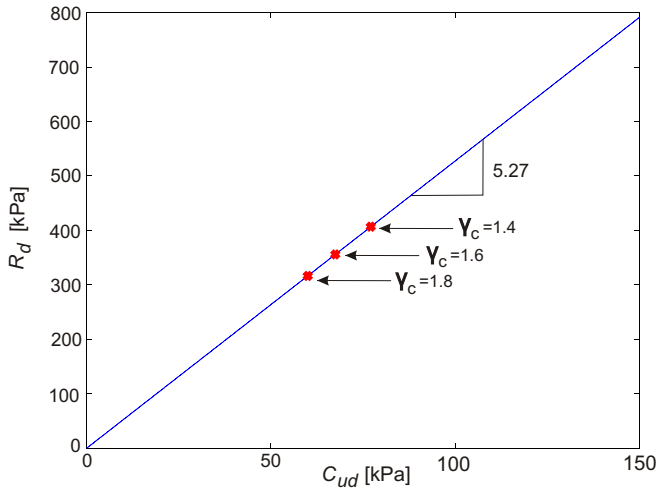

Figure 6.5: Relation between c_{ud} and R_d.

6.5 Probabilistic Analysis

Based on the matrix decomposition method described in Section 3.2, in order to generate a random field some input parameters are needed, namely its mean, μ, coefficient of variation, COV, its correlation lengths in x- and y direction and the coefficient of correlation between the two random fields, ρ. Table 7.3 shows these input parameters for the undrained shear strength, c_u, and Young's modulus, E, of the footing.

Table 6.2: Input parameters for the footing.

Parameter	Value
μ_{cu} [kPa]	135
COV_{cu} [−]	0.4
μ_E [MPa]	29.7
COV_E [−]	0.4
δ_x [m]	3
δ_y [m]	1
ρ [−]	0.9

Through the analysis 1000 realizations were generated resulting in 1000 bearing capacities. Some examples of the load-displacements curves are shown in Figure 6.6. It can be seen that these reflect the randomness of the soil, as the bearing capacity of the soil is not the same in these cases, as expected.

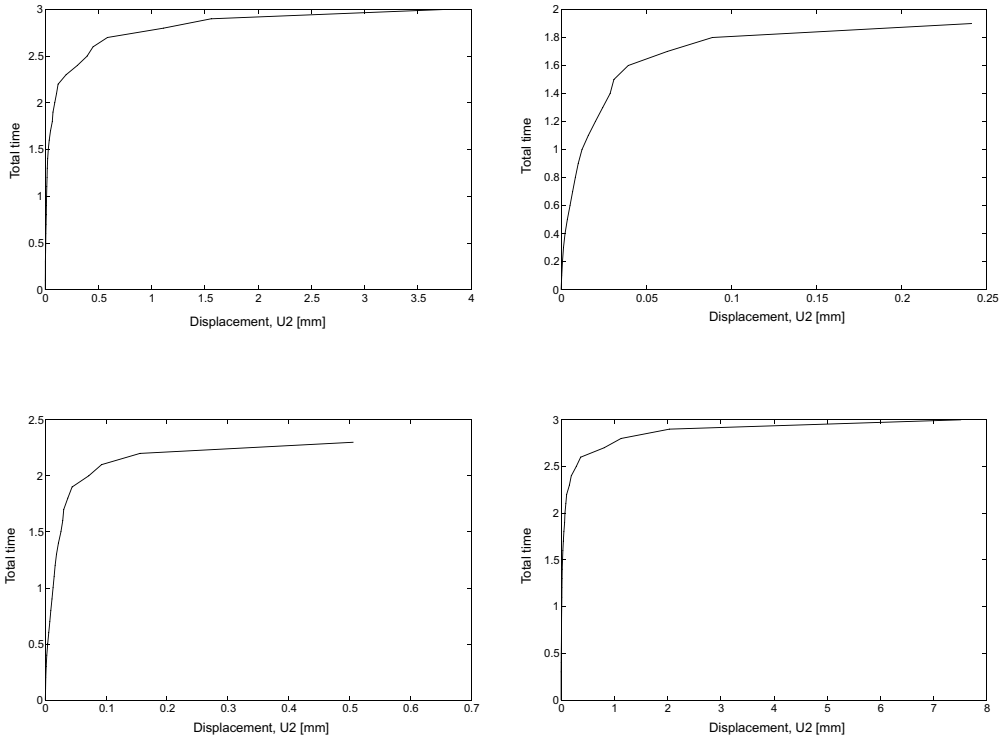

Figure 6.6: Realizations of load-displacement curves.

The data from the Monte Carlo simulations needs to be fitted, so it is important to choose the most accurate distribution, especially at the lower part of the tail. Therefore three types of distributions were fitted to the data, a normal, a lognormal and a Weibull distribution, as seen on Figure 6.7.

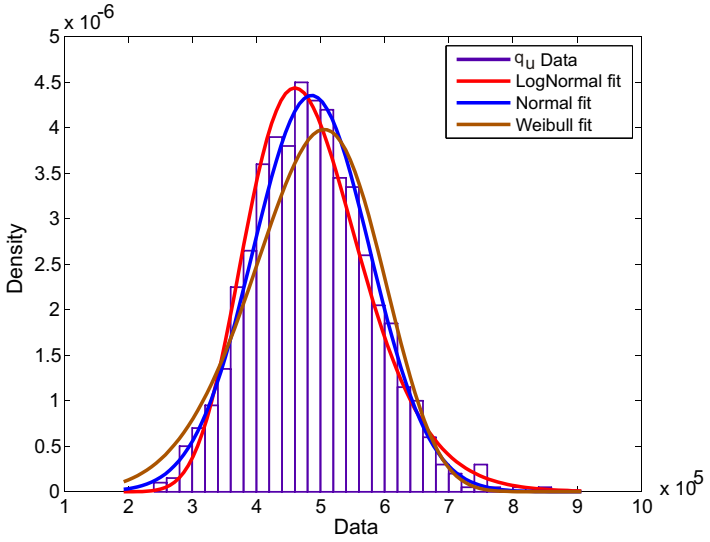

Figure 6.7: Fit for the bearing capacity of the footing.

It can be seen that a normal distribution fits best the data, especially at the lower part of the tail.

6.5.1 Effects of the Correlation Length on the Failure Mechanism

In the following, it is investigated how the different correlation lengths affect the failure mechanism. The correlation lengths have been described in Chapter 3.

In order to do this investigation, three simulations with different correlation lengths in the *x*- and *y* directions have been performed for the footing model. Through these simulations it has been observed that the failure always seeks out the region of the soil with the weakest strength (darker colours). The correlation length gives information about how the soil strengths vary in a particular direction. The larger the correlation length, it is more likely for the soil to have the same strength in that particular direction. How the failure mechanism behaves to different correlation lengths is described through the following realizations of the stochastic soil field.

In the first simulation, as seen in Figure 6.8, the correlation lengths are set to 1 m in *x*- and *y*direction. Based on these correlation lengths, the realization of the stochastic field, as seen in Figure 6.8a, becomes very random, where no layers of different soil strengths can be distinguished. The deformed mesh and the failure mechanism based on this realization is shown in Figure 6.8b and Figure 6.8c, respectively. It can be seen that the failure mechanism seeks toward the left side of the model where the soil has weaker strength. The failure mechanism is based on plotting all mechanical strain rate components (ER).

In the second simulation the generated random field has a correlation length of 5 m in *x* direction and 1 m in *y* direction and is illustrated in Figure 6.9. This shows a more systematic random field, than the previous one. Here the soil region has more of a uniform strength, with less randomness as shown in Figure 6.9a. This is reflected in the deformed shape (Figure 6.9a) and failure mechanism (Figure 6.9c), where the soil moves again towards the weak region, which in this case is a small region under the left side of the footing.

The third simulation is performed with a correlation length of 100 m in *x* direction and 1 m in *y*direction, as seen in Figure 6.10. Having a correlation length approaching a larger number, results in a random field where the soil appears to be homogeneous, as seen in Figure.6.10a. The deformed mesh and the failure mechanism based on these correlation lengths are illustrated in Figure 6.10b and Figure 6.10c. As expected, the failure mechanism is almost symmetrical and resembles very much the failure mechanism by Terzaghi, which was presented in Figure 6.2.

The Matlab and Python scripts together with the FORTRAN subroutines which were used to create the probabilistic model of the footing can be found in *Calculation/Footing/ProbabilisticModel* on Appendix CD.

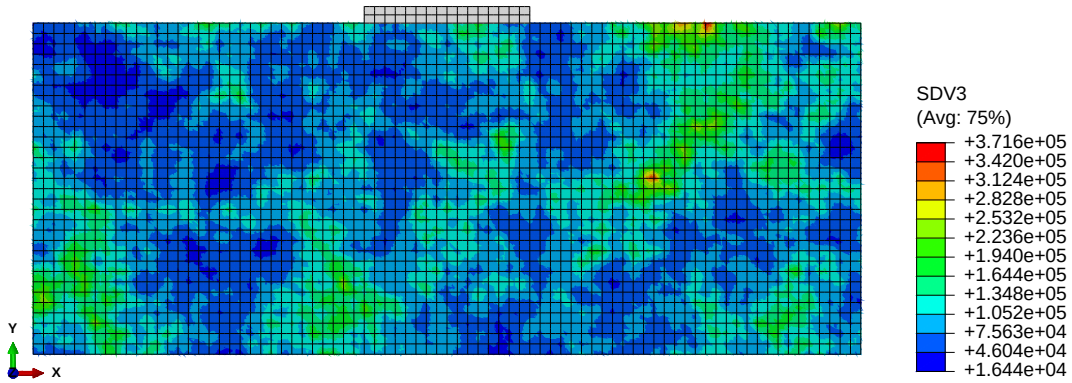

(a) Random field for the undrained shear strength [Pa] with $\mu_{cu} = 135\,\text{Pa}$ and $COV_{cu} = 0.4$.

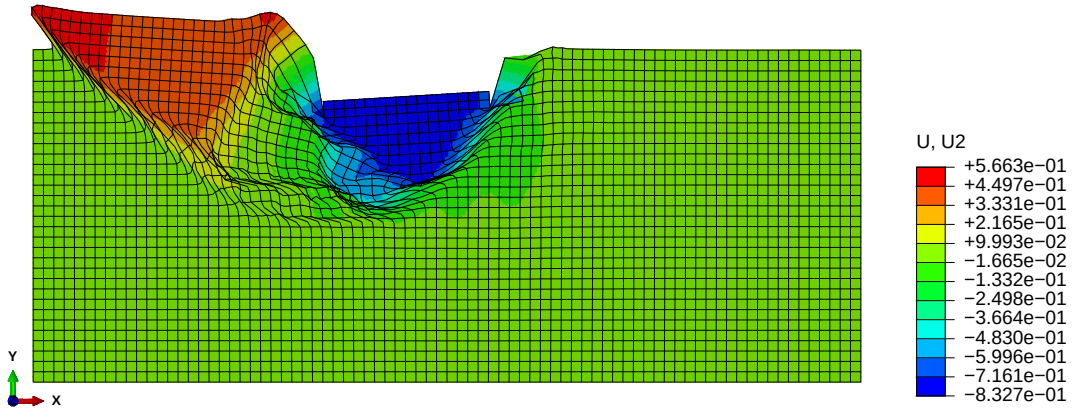

(b) Displacements in the y direction, deformed mesh [mm].

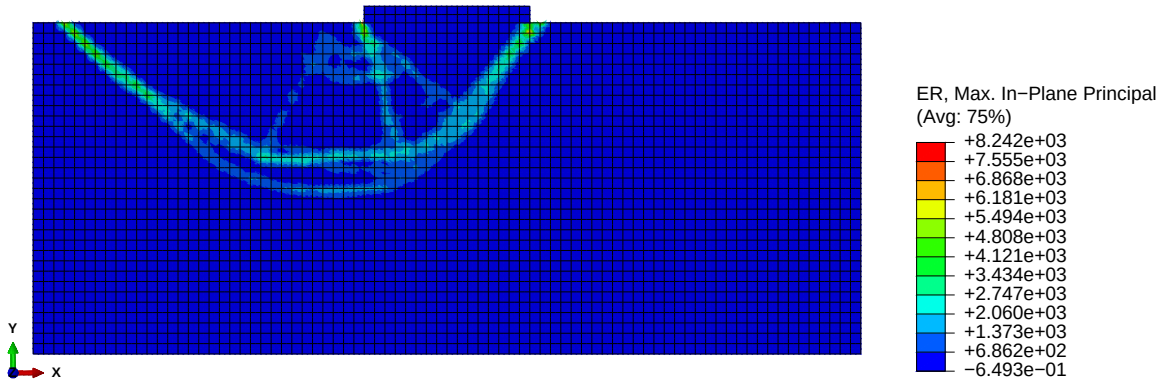

(c) Failure mechanism.

Figure 6.8: Simulation 1 with $\delta_x = 1\,\text{m}$ and $\delta_y = 1\,\text{m}$.

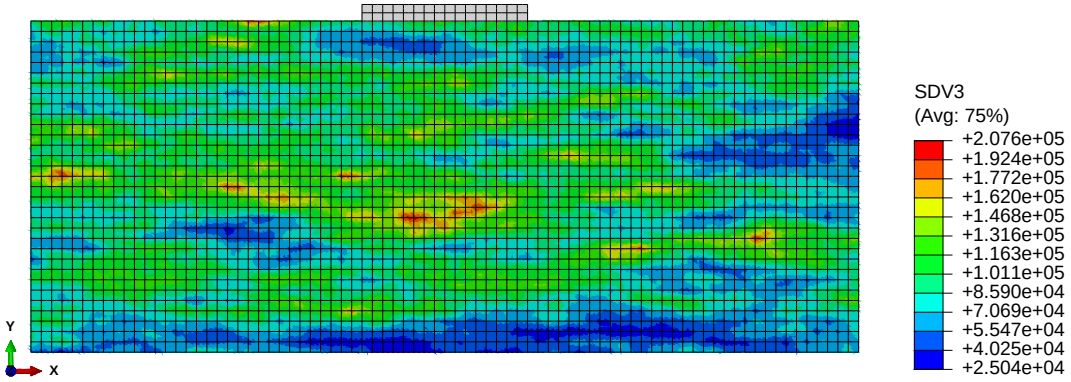

(a) Random field for the undrained shear strength [Pa] with $\mu_{cu} = 135\,\text{Pa}$ and $COV_{cu} = 0.4$.

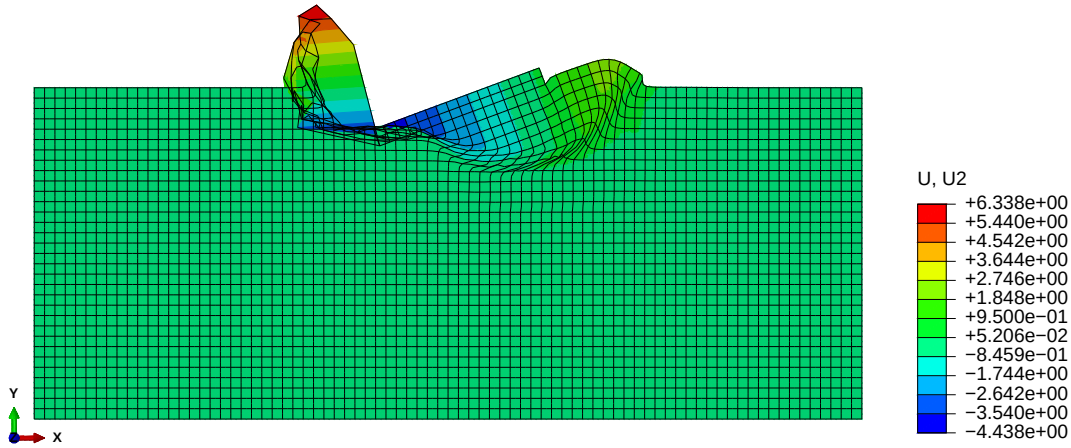

(b) Displacements in the y direction, deformed mesh [mm].

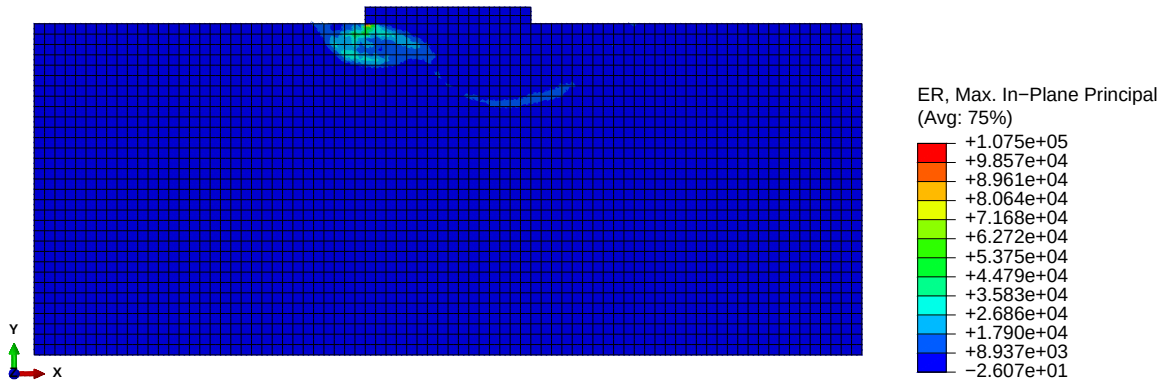

(c) Failure mechanism.

Figure 6.9: Simulation 2 with $\delta_x = 5\,\text{m}$ and $\delta_y = 1\,\text{m}$.

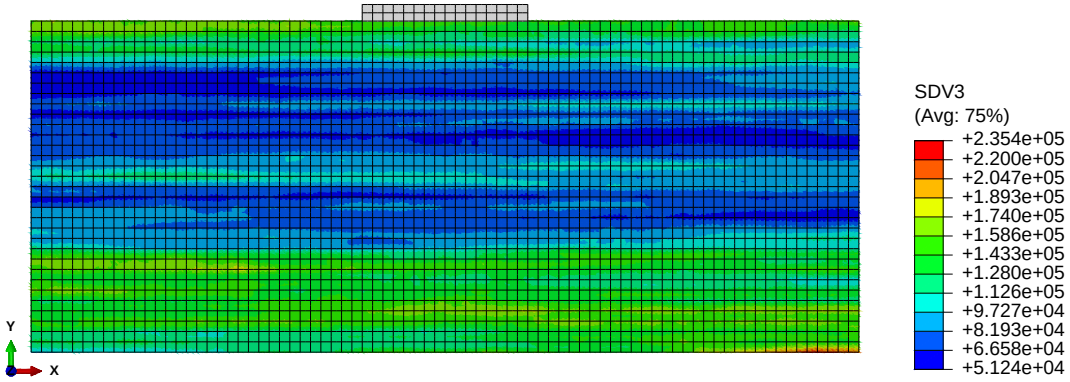

(a) Random field for the undrained shear strength [Pa] with $\mu_{cu} = 135\,\text{Pa}$ and $COV_{cu} = 0.4$.

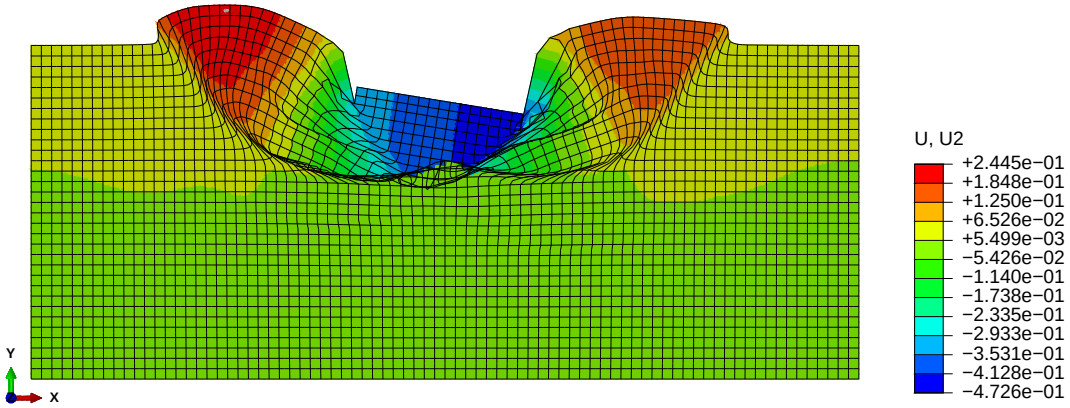

(b) Displacements in the y direction, deformed mesh [mm].

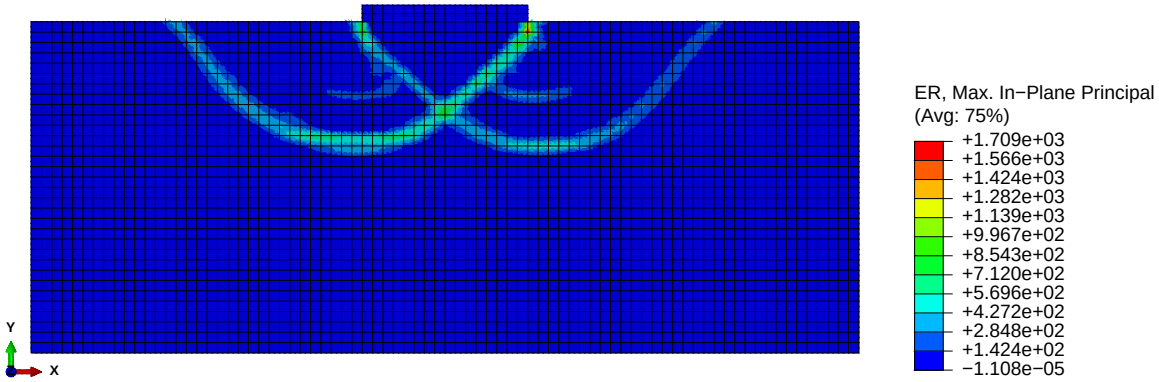

(c) Failure mechanism.

Figure 6.10: Simulation 3 with $\delta_x = 100\,\text{m}$ and $\delta_y = 1\,\text{m}$.

6.6 Reliability Analysis

Through the reliability analysis it is desired to calibrate the partial safety factor for the undrained shear strength until it reaches/comes as close as possible to a target reliability, which for the footing was set to 3.7, corresponding to an annual probability of failure of 10^{-4}.

The results based on the crude Monte Carlo simulation technique, are presented in Table 6.3.

Table 6.3: Calibration of the partial safety factor for the footing - Crude Monte Carlo Simulation.

γ_{cu}	Normal		Lognormal		Weibull	
	β	P_f	β	P_f	β	P_f
1.8	4.00	$3.10{\cdot}10^{-5}$	4.50	$3.44{\cdot}10^{-6}$	3.56	$1.80{\cdot}10^{-4}$
1.6	3.80	$7.00{\cdot}10^{-5}$	4.30	$8.49{\cdot}10^{-6}$	3.37	$3.69{\cdot}10^{-4}$
1.5	3.70	$1.00{\cdot}10^{-4}$	4.14	$1.69{\cdot}10^{-5}$	3.27	$5.31{\cdot}10^{-4}$
1.4	3.58	$1.73{\cdot}10^{-4}$	4.06	$2.39{\cdot}10^{-5}$	3.15	$8.00{\cdot}10^{-4}$
1.2	3.28	$5.15{\cdot}10^{-4}$	3.70	$1.00{\cdot}10^{-4}$	2.89	$1.90{\cdot}10^{-3}$

It can be seen that through a reliability-based calibration the target reliability is reached with a partial safety factor of 1.5 for the undrained shear strength, when the data is fitted with the normal distribution. Figure 6.11 shows how the area of the overlap increases by decreasing the partial safety factor for the soil, resulting in a higher probability of failure.

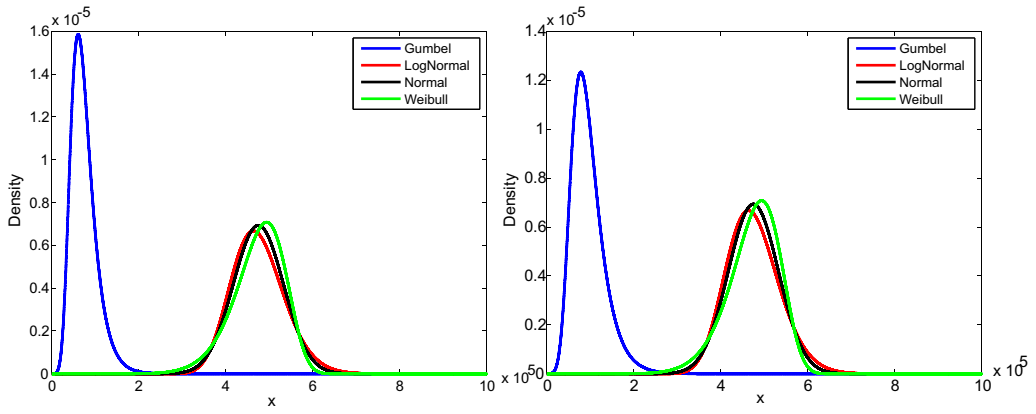

(a) $\gamma_{cu} = 1.8$ (b) $\gamma_{cu} = 1.5$

Figure 6.11: Reliability analysis - Footing.

In addition, FORM was performed too, and the results are shown in Table 6.4.

Table 6.4: Calibration of the partial safety factor for the footing - FORM.

γ_{cu}	Normal		Lognormal	
	β	P_f	β	P_f
1.8	3.60	$1.50 \cdot 10^{-4}$	3.83	$6.38 \cdot 10^{-5}$
1.6	3.38	$3.60 \cdot 10^{-4}$	3.53	$2.00 \cdot 10^{-4}$
1.5	3.25	$5.80 \cdot 10^{-4}$	3.34	$4.20 \cdot 10^{-4}$
1.4	3.11	$9.40 \cdot 10^{-4}$	3.20	$6.87 \cdot 10^{-4}$
1.2	2.75	$3.00 \cdot 10^{-3}$	2.80	$2.54 \cdot 10^{-3}$

It can be seen that by using FORM the partial safety factor cannot be reduced, as the target reliability index is reached with a partial safety factor of $\gamma_{cu} = 1.8$. This is because FORM approximates the failure surface with a straight line, therefore more failures can fall into that.

The calculations and Matlab programme responsible for the reliability analysis of the footing can be found in *Calculation/Footing/ReliabilityAnalysis* on Appendix CD.

CHAPTER 7

Embankment

In this chapter the problem of an embankment will be analysed, where the soil is modelled as a random field. In Denmark some of the embankments for the railways are very old and there is not much data on what type of soils these embankments are consisting of. These embankments consist of different regions with different soil types, but the geometry is not known exactly, just through some certain limits. Therefore creating a probabilistic FE model, where the input and the geometry is automated and it is easy to change, is a good way to analyse the problem. Further in this chapter a reliability analysis is also performed, through which it is desired to calibrate the partial safety factor of the soil strength.

7.1 Problem Definition

The slope and underlying soil is assumed to consist of undrained clay, and the whole model is divided into four different regions to which different material properties are assigned, as seen in Figure 7.1.

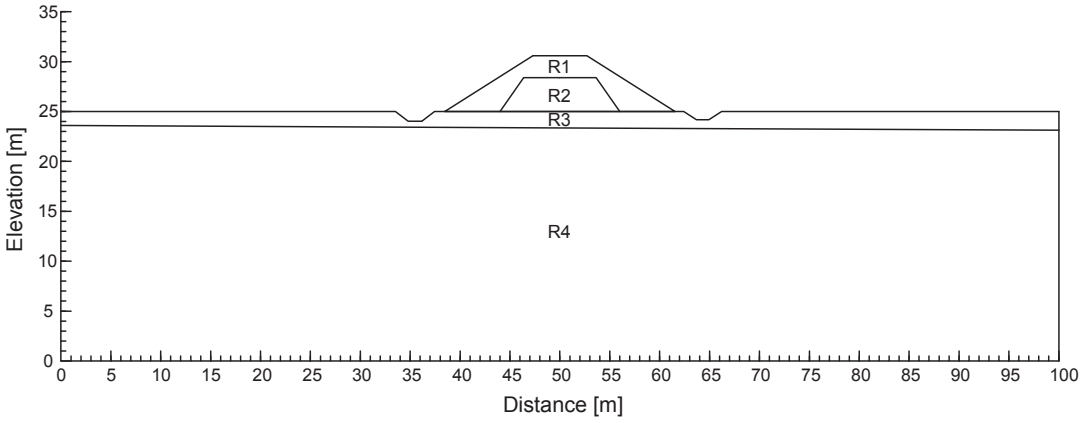

Figure 7.1: The geometry of the embankment problem.

The characteristic value for the different regions are presented in Table 7.1

Table 7.1: Characteristic values of the undrained shear strengthfor the embankment.

Parameter	Region 1	Region 2	Region 3	Region 4
c_{ud} [kPa]	40	70	110	80

In order to analyse this problem the finite element mesh uses a two-dimensional model assuming plain strain. The boundary conditions at the base are restrained in both horizontal and vertical directions, and at the two vertical sides are fixed only in the horizontal direction.

7.2 Convergence Analysis

Just like in the case of the strip footing, a convergence analysis is performed for the bearing capacity of the embankment. The results from the convergence analysis for the footing have shown that the 8-noded elements show better convergence. Therefore, this was adapted and here a convergence has been carried out only with the 8-noded elements (CPE8RH), as seen in Figure 7.2.

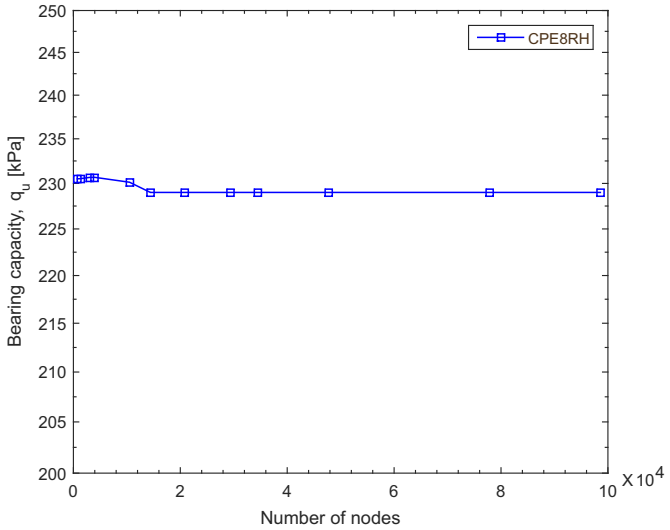

Figure 7.2: Convergence analysis of bearing capacity.

The CPE8RH elements show again good and fast convergence already with 12405 nodes, which corresponds to 4646 elements. This number of elements is adapted and used for the further simulations and calculations.

7.3 Deterministic Calculations

The approach described in Chapter 5 is used in order to find out the design load. Table 7.2 shows the design values of the undrained shear strength, corresponding to the original partial safety factor of $\gamma_{cu} = 1.8$, of the different regions which are used in the deterministic calculations.

Table 7.2: Design values for the embankment.

Parameter	Region 1	Region 2	Region 3	Region 4
c_{ud} [kPa]	22.22	38.89	61.11	44.44

Based on these design values a FE analysis was performed with homogeneous soil, and resulted in a bearing capacity, q_u of 229.6 kPa, which is shown on the load-displacement curve on Figure 7.3. With this the design load, F_d is found as:

$$F_d = 227.3\,\text{kPa}$$

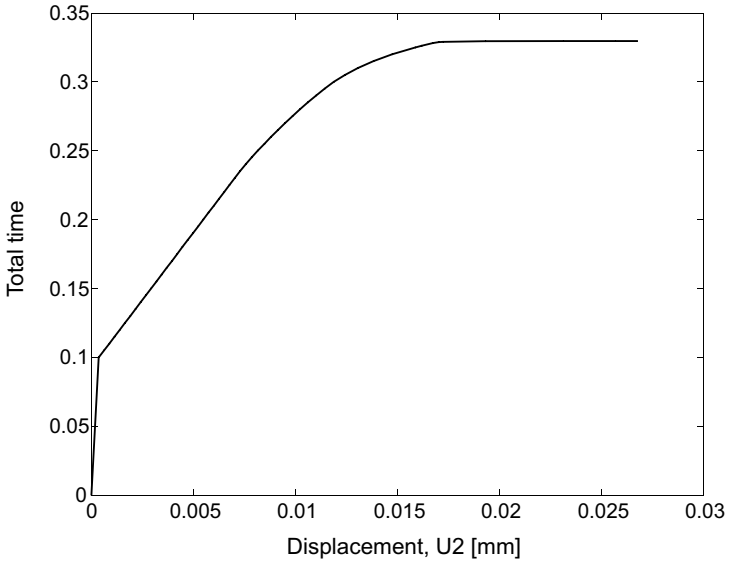

Figure 7.3: Load-displacement curve - deterministic calculation.

The relation between the undrained shear strength, c_{ud}, and resistance, R_d, was investigated, and it was found out that there is again a linear relationship between them, as seen in Figure 7.4

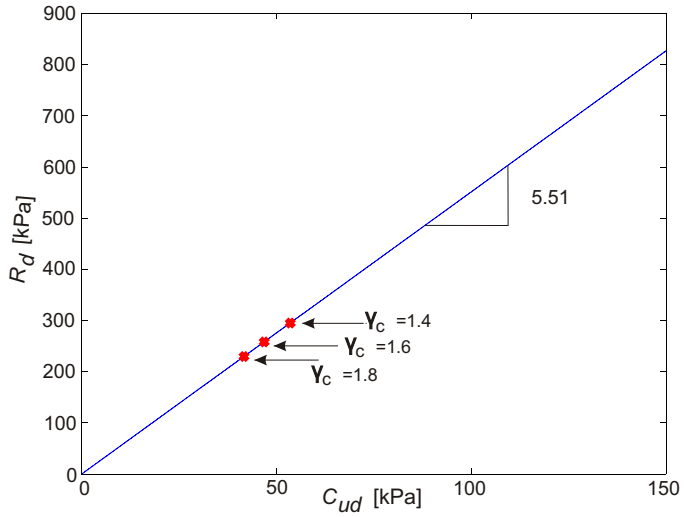

Figure 7.4: Relation between c_{ud} and R_d.

7.4 Probabilistic Analysis

Like in the case of a strip footing, in order to generate the random field for the undrained shear strength, c_u, and Young's modulus, E, some input parameters are needed. These are listed in Table 7.3, together with the unit weight, γ, and Poisson's ratio, ν, for the four different regions.

Table 7.3: Input parameters for the embankment.

Parameter	Region 1	Region 2	Region 3	Region 4
μ_{cu} [kPa]	50	87.5	137.5	100
COV_{cu} [−]	0.4	0.4	0.4	0.4
μ_E [MPa]	29.7	29.7	29.7	29.7
COV_E [−]	0.4	0.4	0.4	0.4
δ_x [m]	0.5	0.5	1	100
δ_y [m]	0.5	0.5	1	1
ρ [−]	0.9	0.9	0.9	0.9
γ [kN/m^3]	18.6	19	21.4	19
ν [−]	0.485	0.485	0.485	0.485

A realization of the generated random field based on the input parameters described in Table 7.3 is shown in Figure 7.5.

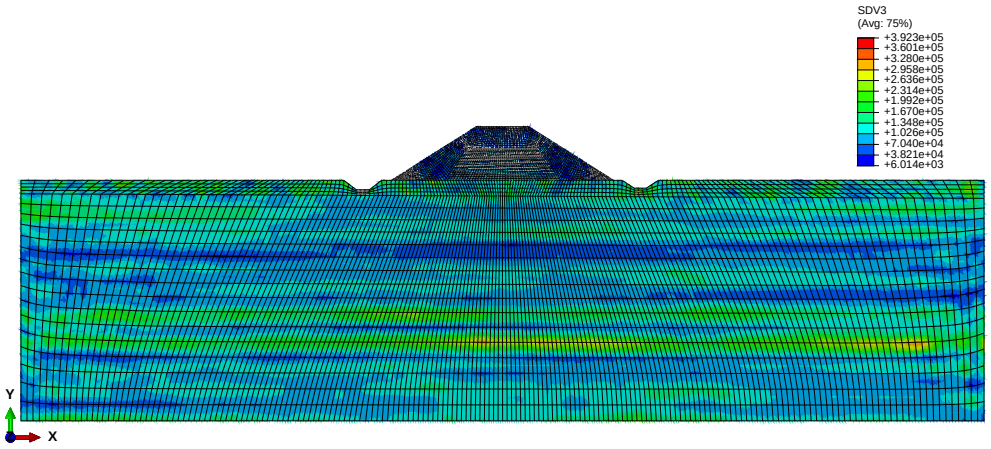

Figure 7.5: Random field for the undrained shear strength [Pa].

In the probabilistic analysis 1000 simulations were performed, resulting in 1000 bearing capacities. As an example, some of the load-displacements curves are illustrated in Figure 7.6.

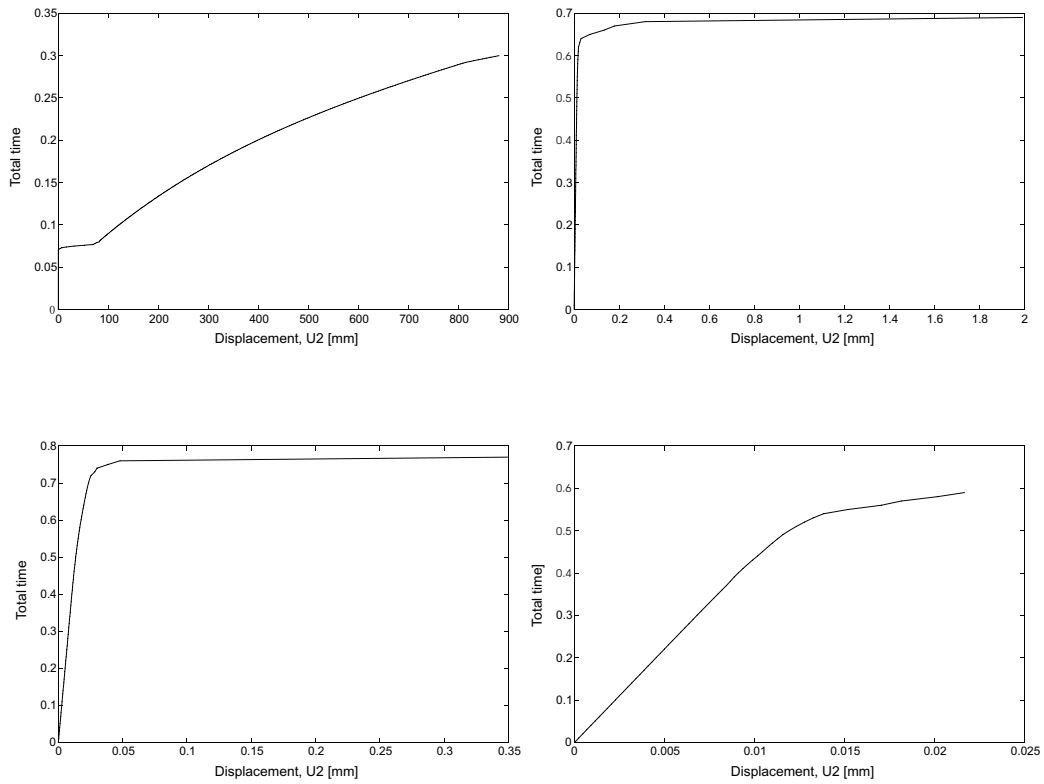

Figure 7.6: Realizations of load-displacement curves.

The data from the probabilistic analysis were fitted to three different types of distributions: a normal, lognormal and a Weibull distribution. The histogram of the sample data of the fitted distributions can be seen in Figure 7.7.

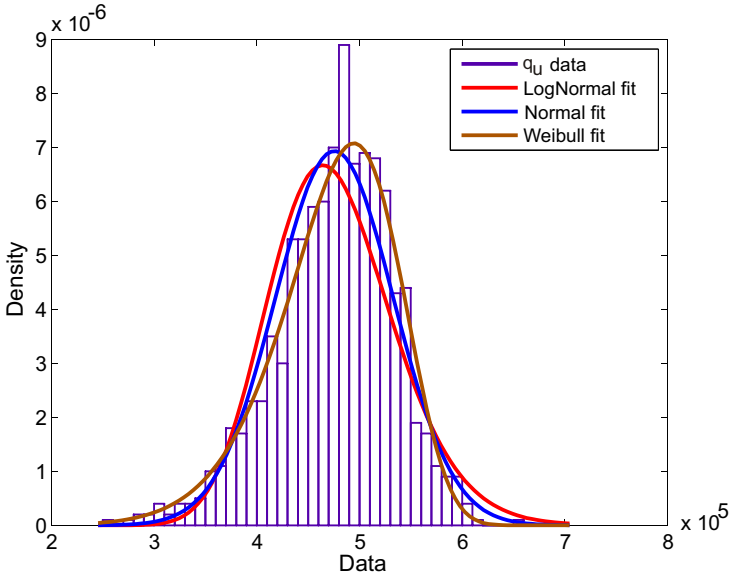

Figure 7.7: Fit for the bearing capacity of the embankment.

It can be seen that the for the embankment the Weibull distribution fits best to the data,

In the following some of the realizations of the probabilistic analysis are shown. Here it should be noted that not the whole models are shown.

The Matlab and Python scripts together with the FORTRAN subroutines which were used to create the probabilistic model of the embankment can be found in *Calculation/Embankment/ProbabilisticModel* on Appendix CD.

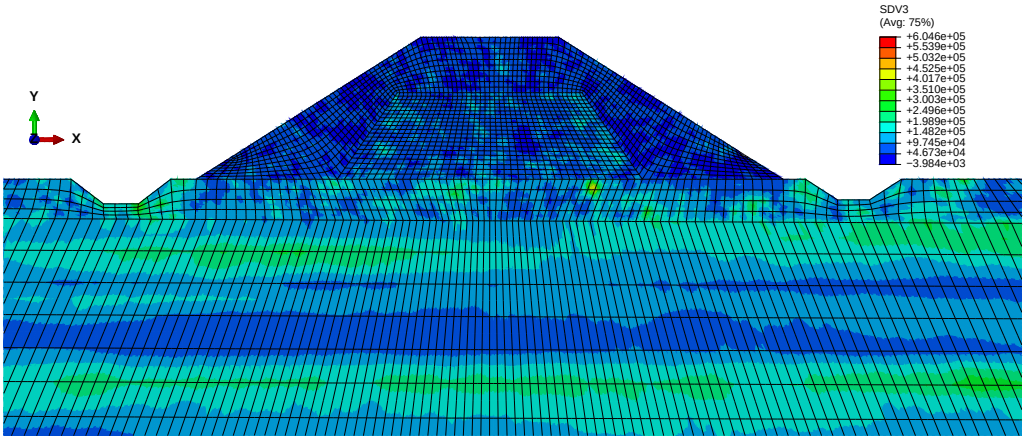

(a) Random field for the undrained shear strength [Pa].

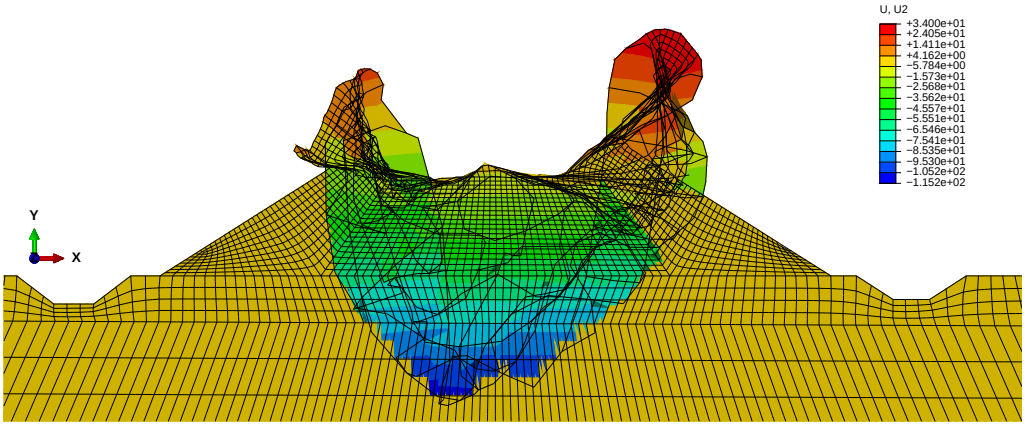

(b) Displacements in the y direction, deformed mesh [mm].

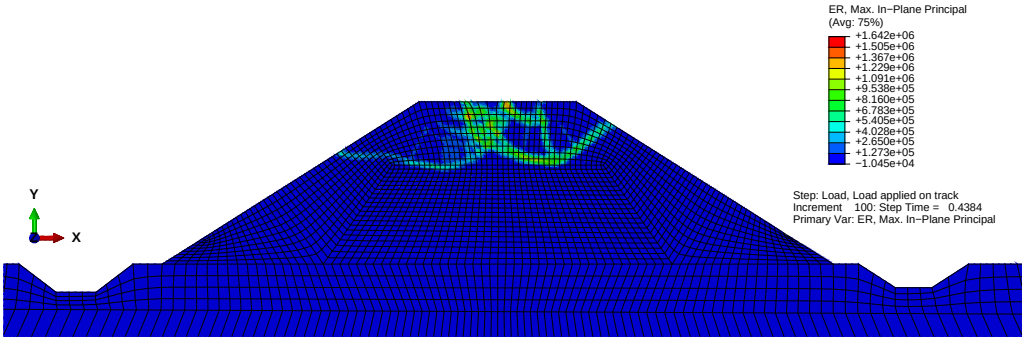

(c) Failure mechanism.

Figure 7.8: Simulation 84.

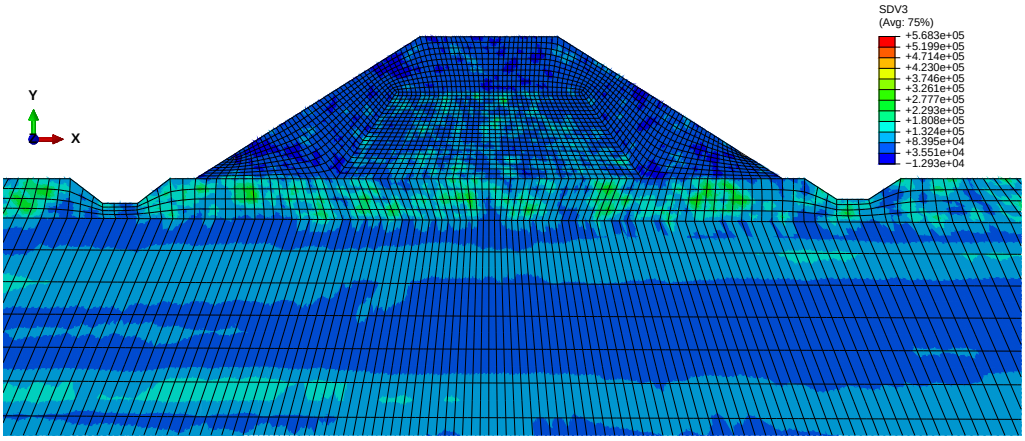

(a) Random field for the undrained shear strength [Pa].

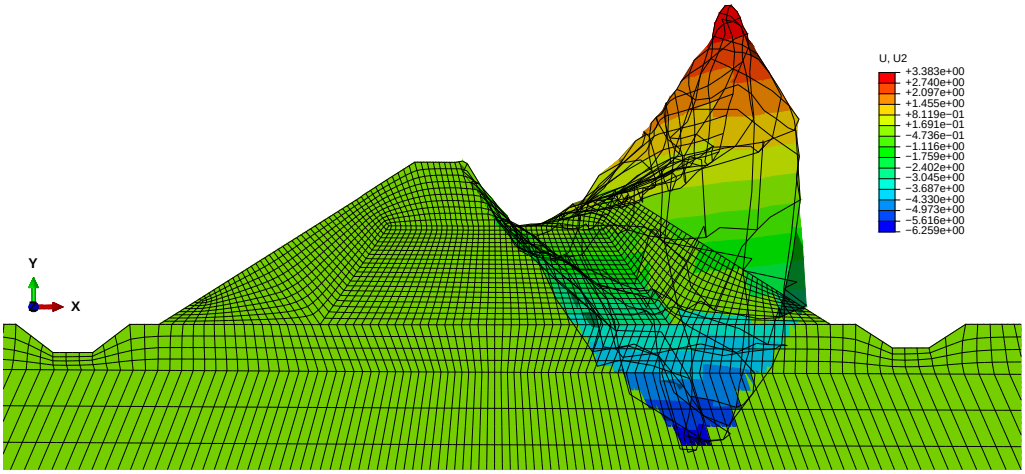

(b) Displacements in the y direction, deformed mesh [mm].

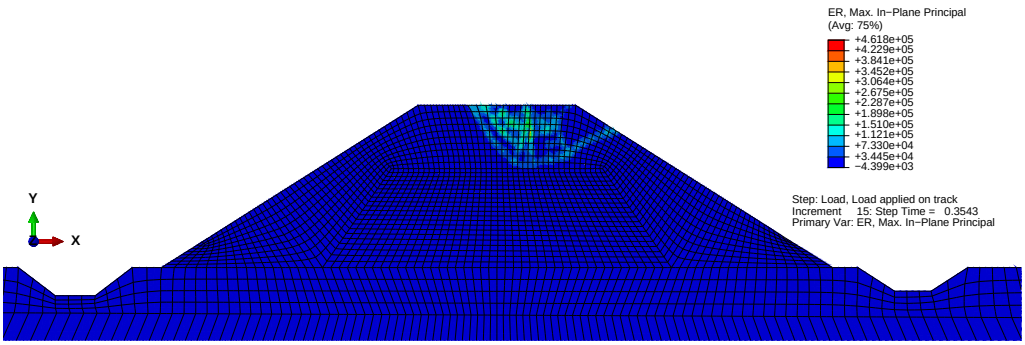

(c) Failure mechanism.

Figure 7.9: Simulation 291.

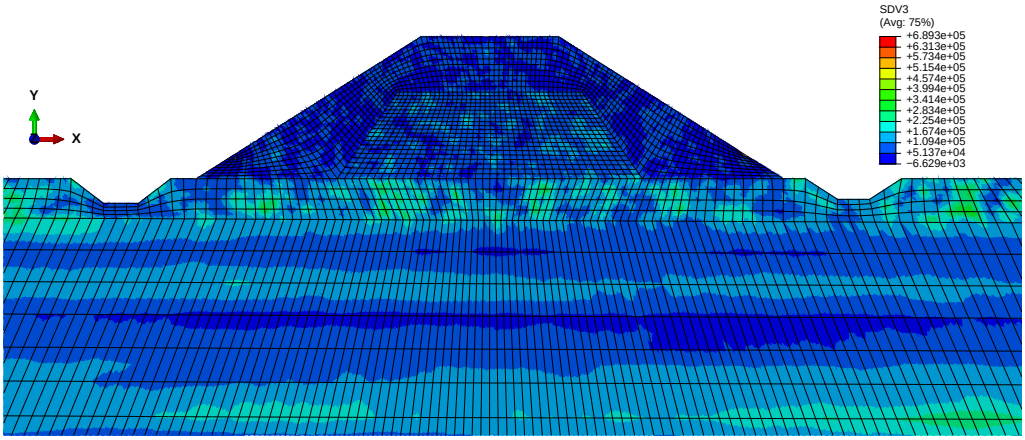

(a) Random field for the undrained shear strength [Pa].

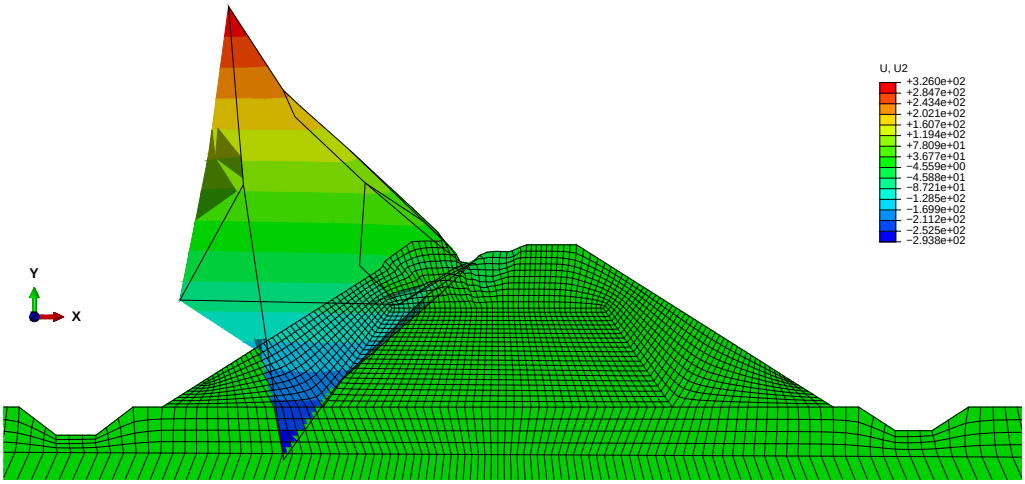

(b) Displacements in the *y* direction, deformed mesh [mm].

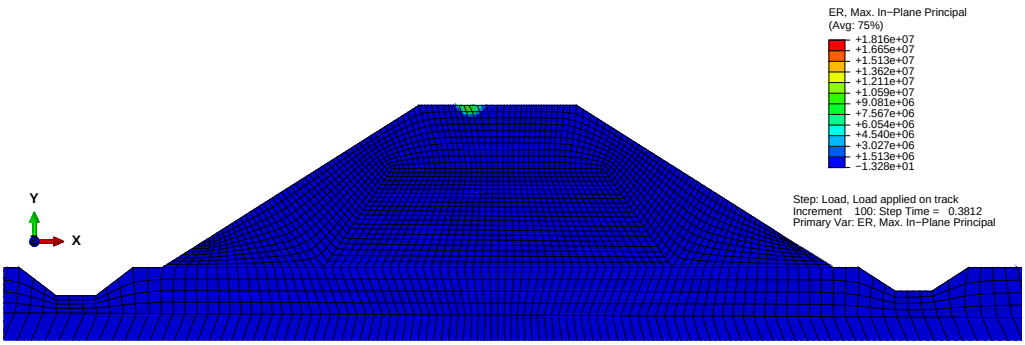

(c) Failure mechanism.

Figure 7.10: Simulation 824.

7.5 Reliability Analysis

Through the reliability analysis it is desired to calibrate the partial safety factor for the undrained shear strength until it reaches/comes as close as possible to a target reliability. For the embankment the target reliability was set to 4.7 which corresponds to an annual probability od failure of 10^{-6}.

The results based on the crude Monte Carlo simulation technique, are presented in Table 7.4.

Table 7.4: Calibration of the partial safety factor for the embankment - Crude Monte Carlo Simulation.

γ_{cu}	Normal		Lognormal		Weibull	
	β	P_f	β	P_f	β	P_f
1.8	6.25	$2.10 \cdot 10^{-10}$	∞	0.00	5.28	$6.23 \cdot 10^{-8}$
1.6	5.44	$2.72 \cdot 10^{-8}$	5.69	$6.40 \cdot 10^{-9}$	4.98	$3.21 \cdot 10^{-7}$
1.5	5.31	$5.50 \cdot 10^{-8}$	5.55	$1.44 \cdot 10^{-8}$	4.88	$5.12 \cdot 10^{-7}$
1.4	4.78	$8.37 \cdot 10^{-7}$	4.81	$7.54 \cdot 10^{-7}$	4.60	$2.07 \cdot 10^{-6}$
1.2	5.00	$2.40 \cdot 10^{-7}$	5.17	$1.16 \cdot 10^{-7}$	4.52	$3.11 \cdot 10^{-6}$

It can be seen that through a reliability-based calibration the target reliability is reached with a partial safety factor of 1.5 for the undrained shear strength, when the data is fitted with the Weibull distribution. As a comparison, the interaction between the load and resistance based on the original and calibrated partial safety factor are shown in Figure 7.11

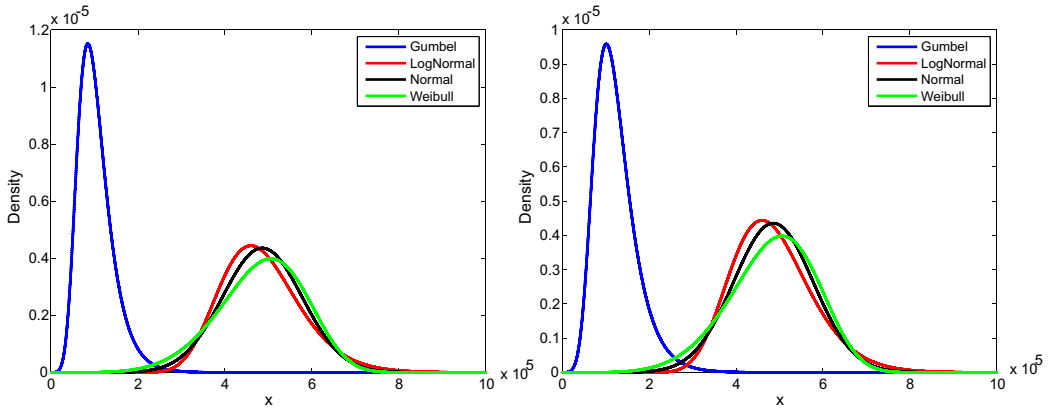

(a) $\gamma_{cu} = 1.8$ (b) $\gamma_{cu} = 1.5$

Figure 7.11: Reliability analysis - Embankment.

FORM was performed in the case of the embankment too, and the obtained results are presented in Table 7.5, showing again conservative results.

Table 7.5: Calibration of the partial safety factor for the embankment - FORM.

γ_{cu}	Normal		Lognormal	
	β	P_f	β	P_f
1.8	4.98	$3.19 \cdot 10^{-7}$	5.03	$2.47 \cdot 10^{-7}$
1.6	4.64	$1.70 \cdot 10^{-6}$	4.67	$1.50 \cdot 10^{-6}$
1.5	4.46	$4.10 \cdot 10^{-6}$	4.48	$3.76 \cdot 10^{-6}$
1.4	4.28	$9.45 \cdot 10^{-6}$	4.29	$9.00 \cdot 10^{-6}$
1.2	4.02	$2.87 \cdot 10^{-5}$	4.03	$2.70 \cdot 10^{-5}$

Another approach was performed, in which the raw data of the bearing capacities were used in the crude Monte Carlo simulation technique. This however resulted in infinite reliability indexes (zero probability of failure). This could be due to the fact that only a limited number of realizations were available and therefore there was no overlap between the histogram of the sample data and the load distribution. This can be seen in Figure 7.12. One way to avoid this is to run more realizations for the bearing capacities, but because of lack of time, this was not possible.

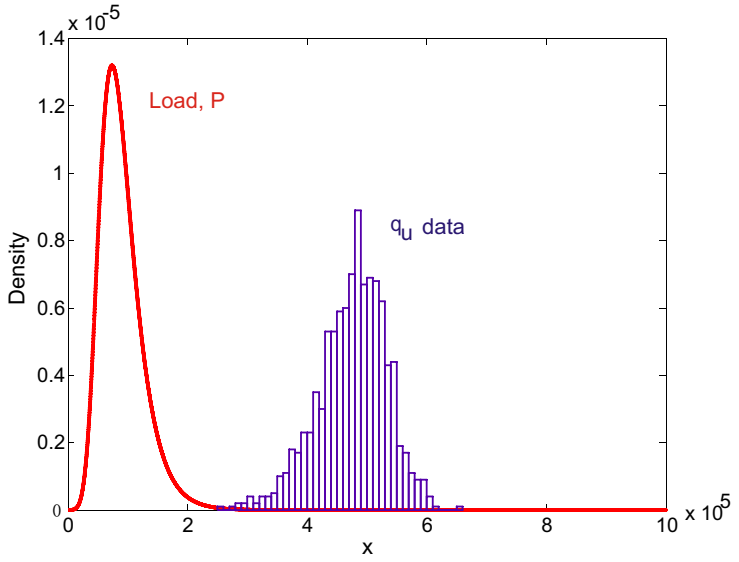

Figure 7.12: Fit for the bearing capacity of the embankment.

The calculations and Matlab programme responsible for the reliability analysis of the embankment can be found in *Calculation/Embankment/ReliabilityAnalysis* on Appendix CD.

CHAPTER 8

Conclusion

The purpose of the thesis was to model the random variations of soil properties by applying the random field theory, and based on that to calibrate the partial safety factor of the undrained shear strength, which in the Danish National Annex to DS/EN 1997-1 [2007] is set to 1.8.

First the different uncertainties related to the geotechnical cases were introduced, from which the main focus was set on the natural soil variability. The natural randomness of the soil was modeled by the use of random field theory, which was described with all the characteristics and assumptions. Two random fields were generated, one for the undrained shear strength and one for the Young's modulus of the soil. For the generation of a two-dimensional random field the matrix decomposition method was used. A probabilistic computational model was constructed using the finite element method, in which the material property in each element was assigned to the generated random field. 1000 simulations were performed, which resulted in a probability distribution of the bearing capacity.

A reliability analysis was performed by the crude Monte Carlo simulation method through which the probability of failure and the reliability index was calculated, based on the interaction between the load and resistance. Thorugh this reliability analysis the partial safety factor for the undrained shear strength was calibrated to a corresponding target reliability index. All these calculations were performed for a strip footing and then for an embankment. It was found that, for both examples, the calculated reliability indices indicate that the partial safety factor can be reduced significantly from the present factor of $\gamma_{cu} = 1.8$ to $\gamma_{cu} = 1.5$.

In addition, it was investigated how the different correlation lengths influenced the failure mechanism of the structure. It was found that for small correlation lengths in the x direction, the failure mechanism was very random. For high correlation lengths, $x = 100\,\text{m}$, the generated failure mechanism resembled very much the failure mechanism by Terzaghi.

In general it is concluded that through a reliability-based calibration, where the uncertainties related to random variations of the soil are accounted for, the partial safety factor of the undrained shear strength can be reduced significantly, by which the costs are reduced too.

8.1 Future Work

The reliability-based calibration of partial safety factors turned out to be efficient. However this was performed only on a fixed coefficent of variation and correlation lengths, due to lack of time. Therefore it would be interesting to perform more simulations with different correlation lengths and coefficient of variation and compare them.

Another limit state equation would be also interesting to investigate. Since cross-correlated random fields were generated between the undrained shear strength and Young's modulus of the soil, this could be used for the serviceability limit state (SLS), where instead of the bearing capacities, the interaction between the load and displacements is analysed.

Bibliography

Element Selection Criteria. URL: http://mashayekhi.iut.ac.ir/sites/mashayekhi.iut.ac.ir/files/u32/presentation10.pdf.

172, **2009**. DS/INF 172. *Baggrundsundersøgelser i forbindelse med udarbejdelse af Nationale Annekser til EN 1990 og EN 1991 – Sikkerhedsformat, lastkombinationer, partialkoefficienter, udmattelse, snelast, vindlast, mm.*, 2009.

1990, **2010**. DS/EN 1990. *Eurocode-basis of structural design*. Copenhagen: Dansk Standard, 2010.

1997-1, **2007**. DS/EN 1997-1. *Eurocode 7: geotechnical designdpart 1: general rules*. Copenhagen: Dansk Standard, 2007.

Abaqus, **2013**. Abaqus. *Abaqus Documentation*. 2013.

Ayyub and McCuen, **2011**. Bilal M. Ayyub and Richard H. McCuen. *Probability, Statistics and Reliability for Engineers and Scientists*. Taylor & Francis Group, 2011.

Azizi, **2000**. Fethi Azizi. *Applied Analyses in Geotechnics*. ISBN: 0-419-25340-8. E FN Spon, 2000.

Banedanmark, **2010**. Banedanmark. *BN1-59-4 belastnings- og beregningsforskrift for sporbærende broer og jordkonstruktioner*. URL:http://www.bane.dk/db/filarkiv/4987/bn1-59-4.pdf, 2010.

C.Fitzjohn, Ternan, Williams, Perez-Gonzales, and Alba, **2002**. C.Fitzjohn, J. L. Ternan, A. G. Williams, A. Perez-Gonzales, and S. De Alba. *Dealing with soil variability: some insights from land degradation research in central Spain*. 2002.

Clausen, Damkilde, and Andersen, **2007**. Johan Clausen, Lars Damkilde, and Lars Andersen. *An efficient return algorithm for non-associated plasticity with linear yield criteria in principal stress spaces*. 2007.

Davidović, Prolović, and Stojić, **2010**. Nebojša Davidović, Verka Prolović, and Dragoslav Stojić. *Modelling of soil paraneters spatial uncertainty by geostatistics*. 2010.

DNV, **2012**. DNV. *Statistical Representation of Soil Data, DNV-RP-C207*. URL: https://exchange.dnv.com/publishing/codes/docs/2012-01/RP-C207.pdf, 2012.

Fenton and Griffiths, **2008**. Gordon A. Fenton and D.V. Griffiths. *Risk Assessment in Geotechnical Engineering*. John Wiley & Sons, Hoboken, New Jersey, 2008.

JCSS-C1, **2006**. JCSS-C1. *Probabilistic Model Code, Section 3.7: Soil Properties*. 2006.

Krabbenhøft, **2002**. Kristian Krabbenhøft. *Basic Computational Plasticity*. Department of Civil Engineering Technical University of Denmark, 2002.

Ovesen, **1995**. NK Ovesen. *Eurocode 7 for geotechnical design*. 1995.

Sarma, Krishna, and Dey, **2015**. C.P. Sarma, A. Murali Krishna, and A. Dey. *Probabilistic slope stability analysis considering spatial variability of soil properties: Influence of correlation length*. 2015.

Schneider, **1999**. H.R. Schneider. *Definition and determination of characteristic soil properties*. 1999.

Sørensen, **2011**. John Dalsgaard Sørensen. *Notes in Structural Reliability Theory And Risk Analysis*. 2011.

Student, **1908**. Student. *The probable error of a mean*. 1908.

Vahdatirad, **2014**. Mohammad Javad Vahdatirad. *Reliability-Based Design of Wind Turbine Foundations – Computational Modelling*. 2014.

Appendix

APPENDIX A

Mohr-Coulomb Model

The Mohr-Coulomb model in Abaqus is based on the Mohr-Coulomb model suggested by Coulomb (1776). In this model, the Mohr-Coulomb criterion assumes that the failure is controlled by the maximum shear stress, and that it depends on the normal stress. Furthermore, in this model it is assumed that the failure is independent of the intermediate stress (σ_2). In general, soils would include some small dependence on σ_2, however, the Mohr-Coulomb model is considered to be sufficiently accurate for most applications. Here, the constitutive model uses an elastoplastic model and the yield function includes isotropic cohesion hardening/softening and uses the potential flow which has no corners in the deviatoric stress space.

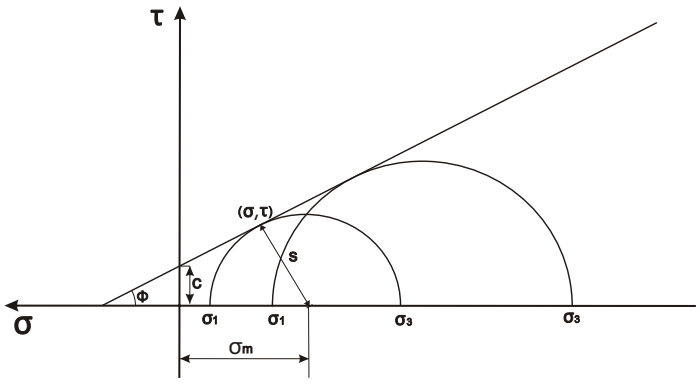

Figure A.1: Mohr-Coulomb yield model.

In Figure A.1 the failure line and Mohr circles are shown, where s is the maximum shear stress and it is half of the difference between the maximum and minimum principal stresses, σ_1 and σ_3 respectively. σ_m is the normal stress which is defined as the average of σ_1 and σ_3. The Mohr-Coulomb criterion can be written as in Equation. (A.1).

$$\underbrace{s}_{Max.shearstress} = \frac{\sigma_1 - \sigma_3}{2}$$

$$\underbrace{\sigma_m}_{Normalstress} = \frac{\sigma_1 + \sigma_3}{2}$$

$$\tau = c - \sigma \tan\phi \tag{A.1}$$

τ	shear stress
c	cohesion of material
σ	normal stress
ϕ	friction angle

where,

Form Mohr's circle in Figure A.1, the shear- and normal stress can be expressed as in Equation (A.2) and (A.3).

$$\tau = s\cos\phi \tag{A.2}$$

$$\sigma = \sigma_m + s\sin\phi \tag{A.3}$$

By substituting Equation (A.2) and (A.3) into Equation (A.1), the Mohr-Coulomb criterion can be rewritten as follows:

$$\begin{aligned}
\tau - c + \sigma\tan\phi &= 0 \\
&\Downarrow \\
s\cos\phi - c + (\sigma_m + s\sin\phi)\tan\phi &= 0 \\
&\Downarrow \\
s\cos^2\phi - c\cos\phi + \sigma_m\cos\phi\tan\phi + s\cos\phi\sin\phi\tan\phi &= 0 \\
&\Downarrow \\
s\cos^2\phi - c\cos\phi + \sigma_m\cos\phi\frac{\sin\phi}{\cos\phi} + s\cos\phi\sin\phi\frac{\sin\phi}{\cos\phi} &= 0 \\
&\Downarrow \\
s\cos^2\phi - c\cos\phi + \sigma_m\sin\phi + s\sin^2\phi &= 0 \\
&\Downarrow \\
s(\underbrace{\cos^2\phi + \sin^2\phi}_{=1}) - c\cos\phi + \sigma_m\sin\phi &= 0
\end{aligned}$$

In the end, the Mohr-Coulomb criterion can be written as in Equation (A.4),

$$s + \sigma_m\sin\phi - c\cos\phi = 0 \tag{A.4}$$

A.1 Yielding behaviour

The yield criterion can be described in term of invariants, which is obtained from the Cauchy stress tensor σ_{ij}. It is usually divided into two parts of tensors. The first is the hydrostatic stress or the so called volumetric stress, and it is usually involved when the volume of a body is changing due to the external force. The second one is the deviatoric stress which is typically used in the failure criteria, and it is involved when the body tends to distort due to the external force. The stress tensor may then be expressed as,

$$\begin{aligned} \sigma_{ij} &= \mathbf{S}_{ij} - p\mathbf{I} \\ &\Downarrow \\ \mathbf{S}_{ij} &= \sigma_{ij} + p\mathbf{I} \end{aligned}$$

where,

$\mathbf{S}_{ij}$	deviatoric stress tensor
$p\mathbf{I}$	hydrostatic stress tensor
p	mean stress $p = \frac{1}{3}(\sigma_{11} + \sigma_{22} + \sigma_{33})$
I	identity matrix

The first invariant, I_1 is described by the principal stresses and can be written as in Equation (A.5). The second and third are described in terms of deviatoric stress S and can be expressed as states in Equation (A.6) and (A.7), respectively.

$$I_1 = Tr(\sigma) = \sigma_{11} + \sigma_{22} + \sigma_{33} \tag{A.5}$$

$$J_2 = \frac{1}{2}\mathbf{S}\colon \mathbf{S} = \frac{1}{6}\left[(\sigma_{11} - \sigma_{22})^2 + (\sigma_{22} - \sigma_{33})^2 + (\sigma_{33} - \sigma_{11})^2\right] \tag{A.6}$$

$$J_3 = det(\mathbf{S}) = \frac{1}{3}(\mathbf{S} \cdot \mathbf{S}) : \mathbf{S} \tag{A.7}$$

Furthermore, the equivalent pressure stress, p, the Mises equivalent stress, q and the third invariant of deviatoric stress, r are defined in Equation (A.8), (A.9) and (A.10):

$$p = -\frac{1}{3}\mathbf{I}_1 = -\frac{1}{3}Tr(\sigma) \tag{A.8}$$

$$q = \sqrt{3\mathbf{J}_2} = \sqrt{\left(\frac{3}{2}\mathbf{S} : \mathbf{S}\right)} \tag{A.9}$$

$$r = 3\left(\frac{1}{2}\mathbf{J}_3\right)^{\frac{1}{3}} = \left(\frac{9}{2}\mathbf{S} \cdot \mathbf{S} : \mathbf{S}\right)^{\frac{1}{3}} \tag{A.10}$$

Based on these, the Mohr-Coulomb yield surface from Equation (A.4) can be rewritten as in Equation (A.11),

$$R_{mc}q - p\tan\phi - c = 0 \tag{A.11}$$

where, R_{mc} is the Mohr-Coulomb deviatoric stress and it depends on the deviatoric polar angle Θ defined as Equation (A.13). ϕ is the friction angle of the material or in other

words is the slope of the Mohr-Coulomb yield surface. The Mohr-Coulomb deviatoric stress is defined as in Equation (A.12).

$$R_{mc}(\Theta,\phi) = \frac{1}{\sqrt{(}3)\cos\phi}\sin\left(\Theta+\frac{\pi}{3}\right)+\frac{1}{3}\cos\left(\Theta+\frac{pi}{3}\right)\tan\phi \tag{A.12}$$

$$\cos 3\Theta = \left(\frac{r}{q}\right)^3 \tag{A.13}$$

The Mohr-Coulomb yield surface in the deviatoric plane can be seen in Figure A.2.

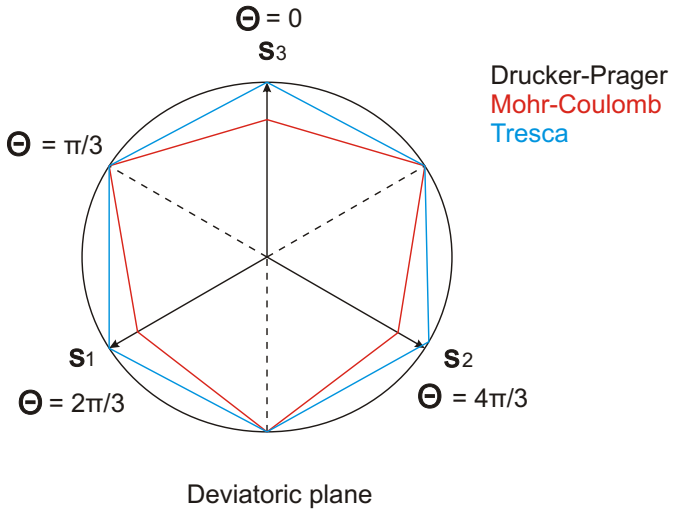

Figure A.2: Mohr-Coulomb yield surface in the deviatoric plane.

A.2 Flow rule

In order to describe the plastic behaviour of the material, the flow rule have to be taken into account. In Abaqus the potential flow is described by Equation (A.14)), where g can be written as in Equation (A.15). The flow potential G is defined in Equation (A.16).

$$d\varepsilon^{pl} = \frac{d\overline{\varepsilon}^{pl}}{g}\frac{\partial G}{\partial \sigma} \tag{A.14}$$

$$g = \frac{1}{c}\sigma : \frac{\partial G}{\partial \sigma} \tag{A.15}$$

$$G = \sqrt{(\varepsilon c|_0 \tan\Psi)^2 + (R_{mw}q)^2} - p\tan\Psi \tag{A.16}$$

where,

$\Psi(\theta, f^{\alpha})$	dilatation angle from meridional plane at high confining pressure
$c\|_0$	initial cohesion yield stress
ε	parameter referred to as the meridional eccentricity

The flow potential, G tends to a straight line in the meridional stress plane as the meridional eccentricity tends to zero as seen in Figure A.3.

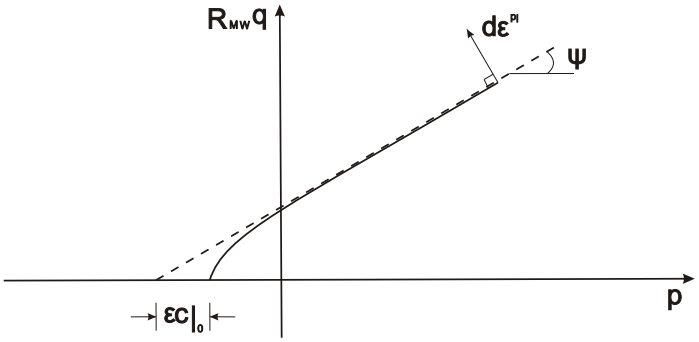

Figure A.3: Hyperbolic flow in the meridional plane

Furthermore, the flow potential, G has a smooth elliptic function (see Equation (A.17)) in the deviatoric stress plane, as seen in Fig. A.4). By using this flow potential, which is continuous and smooth in the meridional stress plane it is ensured that the flow direction is unique.

$$R_{mw}(\Theta, e) = \frac{4(1-e^2)\cos^2\Theta + (2e-1)^2}{2(1-e^2)\cos\Theta + (2e-1)\sqrt{4(1-e^2)\cos^2\Theta + 5e^2 - 4e}} R_{mc}\left(\frac{\pi}{3}, \phi\right) \tag{A.17}$$

Here e is a parameter that describes the "out-of-roundedness" of the deviatoric section and is defined as in Equation (A.18). Alternatively, e can be considered as an independent material parameter, as in Abaqus the value of e can be provided directly. In order to have a convexity and smoothness of the elliptic function, it is required that e is in the range of $(1/2 < e \leq 1)$.

$$e = \frac{3 - \sin\phi}{3 + \sin\phi} \tag{A.18}$$

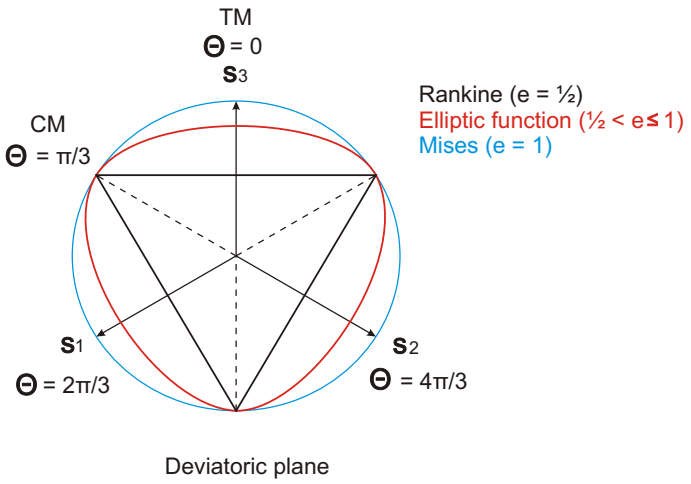

Figure A.4: Flow potential in the deviatoric plane.

The flow potential in the deviatoric plane is illustrated in Figure A.4.

Furthermore, the flow in the deviatoric plane is non-associated and by using this Mohr-Coulomb model, this generally require the solution of nonsymmetric equations.